Measurement Based Vehicle-to-Vehicle Multi-link Channel modeling and Relaying Performance

Xi Chen

Department of Electrical and Information Technology
Lund University

Advisor: Fredrik Tufvesson

December 2015

Printed in Sweden
E-husets tryckeri, Lund, 2016

Abstract

There has been intense research in vehicular communication in order to provide reliable low-latency vehicular communication links for developing intelligent transportation system (ITS). As one of the important properties, vehicle-to-vehicle (V2V) communication is learned to be inherently non-stationary due to the high mobility of both transmitter (TX) and receiver (RX). Therefore, the V2V system behavior is essentially different from previous mobile communication studies and needs to be understood.

For V2V wireless communication systems, it is crucial to model the vehicular channel accurately to evaluate the quality of the system level applications. Among all channel properties in a V2V system, the shadow fading (i.e. large scale fading, LSF) from other vehicles has a significant adverse impact on the system performance. One promising approach to overcome this issue is by implementing multi-hop technology on the vehicular ad hoc network (VANETs). One goal of this thesis report is to implement relaying schemes on simulated Rician channel based on measurements to evaluate the performance of multi-hop technology in V2V systems. Two relaying schemes, Amplify-and-Forward (AF) and Decode-and-Forward (DF), are employed in the bit level simulation. The results of packet error rate (PER) are evaluated together with non-relaying situation for convoy and overtaking scenarios, respectively.

Furthermore, a statistic model is created to model the measured highway environment. Pathloss parameters and shadowing loss together with correlation coefficients are derived. Line-of-sight (LOS) and obstructed line-of-sight (OLOS) conditions are manually separated through on-board video. Each scenario has its own parameter set. Maximum likelihood estimation (MLE) is utilized on the pathloss model to compensate the biasing from the measurement hardware. Also the shadowing is modeled as correlated Gaussian and we derived the decorrelation distance from the auto-correlation function (ACF). The model is also validated against the measurements.

For an ad hoc network, the diversity schemes would be strongly affected by the multi-link correlation. Only a few joint correlation studies for mobile ad hoc network have been made, but rarely for VANETs. The last goal of this report is to study the joint correlation on VANETs based on measurements for four-dimensional position joint correlation model where shadowing is affected by the vehicle distance. To be precise, we focus on the joint correlation of large scale fading affected by the distances between the two receiver vehicles under the same car obstruction. Finally, a stochastic model based on the sum of sinusoids approach is implemented.

Acknowledgements

First of all, I would like to express my sincere appreciation to my supervisor Prof. Fredrik Tufvesson for providing me the great opportunity for this thesis topic. I was more than lucky to have his insightful guidance, endless patience and immense knowledge all the way during the project. It was great pleasure to work under his mentoring.

I am very grateful to Dr. Carl Gustafson and Mikael Nilsson from Volvo cars for their altruistic support and kindness. I would also like to thank my examiner Dr. Fredrik Rusek whose rigorous scientific style enlightens me deeply.

Special thanks to Joao Vieira, Xiang Gao, Xuhong Li and Bei Zhang for their stimulating discussions and warmly encouragement.

I thank all my lecturers and teaching assistants during the two enriched years of master program. Without them it would not be possible to meet the craving for my interest in wireless communication.

Last but not the least, I would like to thank my family and friends in China, for their heartfelt and enduring support from seven hours away.

Table of Contents

Chapter 1

Introduction

1.1 A brief overview of VANETs

Intelligent transportation system (ITS), a crucial component of daily life, has improved people's travelling for over two decades. Since the beginning of the 21st century, there has been an explosive enlargement of the size of the transportation system, which consequently lead to a substantial increase of accidents. The term safety has become number one and essential concept to be improved in the transportation system [1]. As one application branch of the 5G architecture, the ad-hoc vehicle-to-vehicle networks known as VANETs reveal its suitable features.

With the widely use of WiFi technology, the research in Vehicle to Vehicle (V2V) communication was initiated by the Department of Transportation (i.e. DOT) and Crash Avoidance Metrics Partnership (i.e. CAMP). The research effort is known as Dedicated short-range communication (DSRC) which is a WiFi based technology used for vehicle sensors to detect potential collision and threats using the 5.9 GHz band [2]. A large number of V2V studies emerge from there. The idea of VANETs partially come from the similar system of mobile ad hoc network. The idea is that it can provide minimal latency due to a direct communication between vehicles; it is considered to have unlimited power supply since the energy consumption for a vehicle engine is neglectable; The antenna and equipment size will not have the rigorous restriction as for mobile phones and the vehicle-embedded computer can provide ability for calculation and data storage [3].

A VANET is defined as a fast moving outdoor communication network [4]. The communication node typically has a high speed, 20 to 150 km/h. A common single link can have a range up to 1000 meter. The local road environment is relatively stationary and the traffic is considered to have predictable movement pattern since it follows the road. In addition, there could be suitable hosts on the road for information gateways such as traffic lights and gas stations [2]. On the other hand, the network structure is highly dynamic and the communication links often has a very short lifetime. Furthermore, the performance of different links could be highly irregular and could vary from different vehicle types, relative speeds and traffic types, etc [5]. To manage the difference situations in the environment, many specific V2V scenarios are brought up for the research, e.g., highway merging lanes, rural opposite, intersection urban multiple lanes, tunnel convoy, bridge convoy, etc. In the future, more particular sub-scenarios will be specified [2].

In recent years, technologies such as automatic parking, collision avoidance system and automatic driving based on vehicle-embedded sensors gradually have come into the

public eye. These vehicle related technologies provide a very promising path towards safe driving. In regard to this, some people even doubt the necessity of V2V communication. I definitely agree on the point that the on-board-vehicle sensor technologies provide much credible improvement to the safety, however I would like to suggest that the development of V2V network is inevitable. With VANETs, a large number of new applications could be built under the prevalent concept of Internet of things, cloud computing and big data. One can study the traffic pattern with massive real-time information, and effective measures could be taken even before the initial of an accident with the awareness of surrounding traffics.

Moreover, with the mature mesh network technology as basis, such as WCDMA, LTE and WiMAX, VANETs are able to form heterogeneous inter-vehicular networks with the evident benefits of safe driving (collision detection); travel efficiency (path rerouting and accident awareness); energy saving (vehicle platoons), etc.

1.2 Thesis goal

The fundamental limitations of VANET systems are the reliability and latency performance, which are strongly impacted by the properties of the individual wireless communication channels. The communication link can be highly dynamic in nature with high penetration losses, high mobility of vehicles and antennas being close to ground-level [5]. In the literature, V2V communication is described to be inherently non-stationary due to high mobility of both transmitter (TX) and receiver (RX) ends. As a result, the channel models for V2V are essentially different from mobile communication channels that have been studied in the pass century. Channel models specifically designed for V2V are required [2].

One key parameter in V2V channel modeling is the shadowing effect from vehicles, which have a significant adverse impact on the system performance [6]. To overcome the issue, multi-hop technology is believed to be an attractive approach [6]. Therefore, one aim of this report is to evaluate the performance of implementing relaying schemes in V2V systems based on measurements. The shadow fading is found to be correlated and can be modeled with a Gaussian distribution [7]. To study the joint shadowing effect, a statistic model can be created with a pathloss and shadowing model. Two basic scenarios LOS and OLOS are considered during the modeling.

The diversity schemes would be strongly affected by correlation. Most related correlation studies have considered single link while a few studied one to multiple cases or vice versa. Due to the requirement of low latency and accuracy in VANETs, the vehicular multi-link channels demand the consideration of the joint shadowing process [8]. In [9], the correlation of disparate links at a single time is studied with a random obstructions geometry based ad hoc sensor network. In [6], the joint correlation process in mobile ad hoc network (MANET) have been studied with an independent link assumption and a four-dimensional position model is created. For VANETs, one could consider joint correlation from both movement coordinates branch and correlation with geometry based car shadowing. Therefore, the other aim of the report is to investigate the joint correlation of the multi-link shadowing process in VANETs and create a stochastic vehicular shadowing model regarding the channel power spectral density (PSD) and the correlation properties.

1.3 Methodology

This thesis mainly focuses on the car shadowing, affecting the large scale fading (LSF). The evaluation data is based on a measurement campaign performed in April 2014 in a Highway convoy scenario with four Volvo vehicles equipped with synchronized transceivers and specifically designed antennas [6]. Instead of a comprehensive but more complex channel measurements with channel sounders, the data is collected as several sets of RSSI (i.e. receive signal strength indicator) values from each car, and all distances between cars are calculated from GPS coordinates. With on-board cameras, two basic scenarios can be studied separately and compared, i.e. line-of-sight (LOS) and obstructed-LOS (OLOS). The OLOS is such situation where the LOS component is obstructed by nearby objects, e.g., other cars, roadside rails, forest, buildings, traffic signs, trucks and bridges [6]. On one hand, V2V could particularly beneficial on OLOS situations by introducing extra multi-path components from diversity point of view. On the other hand, due to the obstruction of LOS, additional propagation losses are induced and would result in reduction of the communication range [5].

Two relaying schemes Amplify-and-Forward (AF) and Decode-and-Forward (DF) [10] are implemented to simulate and evaluate the multi-hop performance on V2V system. Random packets with size 100 bytes are generated with proper coding and passed on to the simulated channel on a bit level. Each measured RSSI value is modified as average transmit power for one packet transmission and simulated as Rician channel on a bit level. Maximum ratio combining (MRC) is adopted for both relaying schemes at destination receiver for diversity combining [11]. Eventually, the performance of packet error rate (PER) is analyzed for both scenario convoy and overtaking.

In the second part of the report, a pathloss model is created based on the measurements data with single-slope regression. Maximum likelihood estimation (MLE) is employed to compensate the limitation of hardware biasing [12]. Large scale fading is derived by subtracting the local power mean calculated from linear regression. It is later analyzed to be zero mean and we calculated its standard deviation. The decorrelation distance can be calculated from the auto correlation function (ACF) of the shadowing and is used to simulate large scale fading exploiting a correlated Gaussian process. Finally, the resulting channel is evaluated and compared with the simulation results.

In the last part of the report, a stochastic model based on the sum of sinusoids approach is employed with Monte Carlo simulations to simulate the joint correlation process. The decorrelation distance of the shadowing is studied to decide the joint correlation parameter regarding the effect of movement coordinates. Furthermore, the joint shadowing influenced by different distance from TX to Rx is also studied and the correlation coefficient for different distances between cars are derived. Furthermore, with the Gaussian process shadowing auto-correlation assumption and the Gudmundson model, the joint correlation can be modeled as a negative exponential function [5]. The power spectral density (PSD) of the shadowing process is estimated with the joint correlation parameters which is used to generate the spatial frequencies in sum of sinusoids model. At last, the final model as joint shadowing regarding both position and distances between cars would have a close correlation properties with measurements [8].

1.4 Contribution

The main contributions of this thesis report are:

- The Decode-and-Forward and Amplify-and-Forward relaying simulation results based on measurements shown in Figure 3.6, 3.7 and Table 3.1, 3.2 indicate that the multi-hop techniques provide an efficient way to overcome the car-shadowing issue in V2V systems.
- A statistical model with pathloss model illustrated in Figure 4.2 and correlated Gaussian large scale fading described in equation (2.15) is created for highway scenario regarding the line-of-sight and obstructed-line-of-sight situations.
- Using the sum of sinusoids approach described in equation (2.32), realistic V2V multi-link stochastic channels with desired power spectral density and correlation properties could be generated for network simulations and system testing.
- The joint correlation of large scale fading affected by the distance between two cars of a multi-link with same car obstruction is studied and added to the sum of sinusoids based stochastic model. Simulation of the vehicular shadow fading is demonstrated in Figure 5.9.

1.5 Outline

This thesis report is organized with three major parts following the three goals. In Chapter 2, basic principles of V2V channel modeling, relaying and the approach of sum of sinusoids are introduced. The setup of the measurements and data processing are also presented here. In Chapter 3, after a short introduction of the simulation system, the detailed results of Decode-and-Forward and Amplify-and-Forward relaying schemes are illustrated and compared together with non-relaying both for scenario convoy and scenario overtaking. Chapter 4 outlines the statistic pathloss shadowing model with maximum likelihood estimation and correlated Gaussian. Packet error rate results are also evaluated here. In Chapter 5, the joint correlation of two links is studied regarding position and influence of different distances between cars. The results of the stochastic sum of sinusoids model are evaluated. Finally, the conclusion and discussion are presented in Chapter 6 and Chapter 7.

Chapter 2
Background Theory

2.1 Vehicle to Vehicle channel

In wireless communication, the electromagnetic waves propagate from the transmitter to the receiver over an air-interface, called propagation channel. Unlike wired systems, the nature of the channel is dependent on the environment. With the fact of that, the performance of a wireless system is ultimately defined by the properties of the propagation channel, which is extremely important to be understood and modeled. [11]

2.1.1 Channel model

The term channel modeling is used to characterize the effects of the studied channel with understanding and quantifying its behavior for network simulations and system testing. There are various approaches to model a channel regarding the desired properties. For example, a channel can be modeled as time invariant or time varying, which is defined by whether the impulse response is dependent explicitly on time; It could also be studied as narrowband or wideband with regard to the frequency being flat or selective; Taking the antenna diversity into consideration, it can be single-input single-output (SISO) or multi-input multi-output (MIMO); Based on whether there is comprehending continuous knowledge of the environment, a channel could also be modeled as deterministic or stochastic [5].

The vast majority of V2V channels are considered to be linear time-variant systems (LTV) where the impulse response changes with time due to the variability of the channels [5]. This is conclusive, since in V2V systems, the TX and/or RX vehicles are typically moving fast together with the changing of the environment during the communication. Furthermore, due to the uncertainty of the route, it is neither typical nor sufficient to model the vehicular channel from a deterministic point of view which would require the exact locations of the TX, the RX and at least all the major scatterers in the environment. Regarding to that, a general V2V propagation channel could be modeled stochastically.

In a stochastic channel model, the statistics of the channel parameters are normally reproduced with a probability density function. Some of commonly used parameters are discussed in the following. The average power delay profile (PDP) and the power spectral density (PSD) describe the expected received power over a certain time window and over a certain delay respectively. By integrating the PDP over all delays (i.e. the zero order moment of PDP), a single parameter is obtained, known as channel gain, which is be the

major parameter analyzed in this thesis. Furthermore, a normalized second order central moment of the average PDP and the PSD can be used to describe the instantaneous RMS delay spread and the Doppler spread respectively. These two variables can be used to estimate the coherence bandwidth B_c and coherence time T_c, which evaluate the frequency selectivity and time selectivity of the channel respectively. In this thesis, the coherence time T_c of the large scale fading is evaluated by calculating the processed auto correlation within an observation region and defining as the result time duration where the correlation drops from the peak to half. [11] [5]

To model the propagation channel as a stochastic time-variant system, a multidimensional probability density function of the channel impulse response would be needed. An impulse response is the result of the superposition of all the line-of-sight and scattered multipath components at a certain instant. In practice, it is not feasible to derive the multidimensional probability density function in V2V systems. Therefore, an auto correlation function (ACF) is used as an alternative, which is a second order description of the system function [11]. The ACF is obtained by multiplying the system function with its complex conjugate and then taking the expectation $E\{\cdot\}$ over the ensemble of the channel realizations [13]. This is further discussed in the spatial correlation subsection 2.1.6.

In order to simplify the complexity of the channel characterization, many wireless channels are modeled using a wide sense stationary uncorrelated scattering assumption, i.e. WSSUS. The WSS implies that the contribution from different delays are uncorrelated, i.e. the second order statistic channel correlation function depends not on the absolute time but only on the difference of time. The US implies that the scatterers with different path-delays are uncorrelated, i.e. the second order statistic channel correlation function depends not on the absolute frequency but only on the difference of frequency [11]. The WSSUS assumption effectively simplifies the characterization of the channel and still being able to accurately describe its properties. However in general, V2V channels do not qualify the WSSUS assumption due to the fast movements of both the TX and RX together with the changing of environment scatterers. To avoid being entangled with massive complexity, the non-WSSUS V2V channels are treated as an extension of the WSSUS assumption. It is assumed that any region of the vehicular fading process represents the average statistical properties of the entire process (i.e. an ergodic process). Then within certain observation region, the V2V channel could be considered as WSSUS qualified [6].

Additionally, the V2V channel parameters used in this thesis are all refer to SISO channel, since the focus of this thesis is not on antenna diversity.

2.1.2 Pathloss and shadowing Model

Pathloss is the expected power loss at a certain distance compared to the receive power at a reference distance. Together with the shadow fading (i.e. large scale fading, LSF) and the multipath fading (i.e. small scale fading), the signal propagation over the wireless channel can be described. In this thesis, the multipath fading is not the primary interest, and it is removed from the measurements by employing a sliding window. The antenna gain and the system loss are also removed manually from the measurement data. Therefore, in the dB domain, the relation of received signal power $P_{\mathrm{RX}}(d)$ at RX regarding the distance d from TX, the transmitted power (P_{TX}), the mean pathloss $\overline{PL(d)}$ together with the *LSF* can be expressed as [5],

$$P_{\mathrm{TX}} = P_{\mathrm{RX}}(d) + \overline{PL(d)} + LSF. \tag{2.1}$$

In general cases, a simple log-distance power law is used to model the mean pathloss. Together with the large scale fading, the pathloss shadowing model expression in dB domain can be written as, [12]

$$PL(d) = PL_0 + 10n\log_{10}\left(\frac{d}{d_0}\right) + \Psi_\sigma, \tag{2.2}$$

where PL_0 is the pathloss at reference distance d_0 in dB and d is the distance between TX and RX. n is the pathloss exponent, which is an environment dependent parameter provided by measurements. Ψ_σ is a random variable which describes the large scale fading around the distance dependent mean pathloss, which can be modelled by a Gaussian distribution with zero mean and environment determined standard deviation σ. The reference value PL_0 could theoretically be modeled based on the free space pathloss as, $PL_0 = 20\log_{10}(\frac{4\pi d_0}{\lambda})$, where λ is the wavelength of carrier frequency. This method of calculating the reference power only valid for LOS scenarios, for OLOS scenarios, it is obvious that free space condition does not hold due to the obstructions. Hence in this report, the term PL_0 is determined on the estimation from measurements data [5].

In addition to that, refer to the pathloss of LOS scenario only, a dual-slope model based on two-ray ground model could represent measurements data more accurate as the power decay could differ after a certain distance,

$$PL(d) = \begin{cases} PL_0 + 10n_1\log_{10}\left(\frac{d}{d_0}\right), & if\ d_0 \le d \le d_b \\ PL_0 + 10n_1\log_{10}\left(\frac{d}{d_0}\right) + 10n_2\log_{10}\left(\frac{d}{d_b}\right). & if\ d > d_b. \end{cases} \tag{2.3}$$

A piecewise linear model is created with the assumption that the power decays with a pathloss exponent n_1 until the break-point distance d_b and then it decays with a second pathloss exponent n_2. The break-point distance d_b in a typical flat earth model is considered as the distance of which the first Fresnel zone touches the ground. d_b can then be calculated as, $d_b = \frac{4h_{\mathrm{TX}}h_{\mathrm{RX}} - \frac{\lambda^2}{4}}{\lambda}$, where λ is the wavelength at carrier frequency f_c, which in this case is 5.9 GHz, and h_{TX} and h_{RX} are the height of TX and RX antennas to ground, respectively [11]. In V2V communication systems, the TX and RX heights are typically very low. In this report, h_{TX} and h_{RX} are treated the same, approximately 1.5 meter. After calculation, the break-point distance d_b for this measurements is approximately 180 meter.

The dual slope characteristic mainly comes from the additive and subtractive combination of the LOS wave and reflect ground wave [14]. Before the break-point distance, a multi-ray behavior can be observed accordingly and after the distance extend over break-point distance, the two waves are always combined subtractively resulting a faster power loss. With respect to that, the dual slope could be easily justified for a LOS scenario. However, in an OLOS scenario, neither of the two waves should theoretically follows a clear pattern and the validation of the dual slope model needs more consideration. In this thesis report, only one pair of exponent and reference value is extracted for each LOS and OLOS scenario as equation (2.2).

2.1.3 Shadowing

The large scale fading describes the losses as the wireless signal propagates through or around major obstructions in its path between TX and RX. The shadowing is derived by subtracting the average RSSI values from the distance dependent estimated pathloss. The estimation of the pathloss coefficient is based on the measurements data with linear regression and Maximum-likelihood estimation (MLE) [12]. As the V2V multi-link shadowing is under a non-stationary situation, in order to study it, one can consider the shadowing as a stationary process within certain time period (i.e. traveled distance), which refer to the decorrelation distance determined from shadowing auto correlation function [13]. In this work sliding window is employed on the RSSI values before the subtraction, i.e. one second window of moving average over ten consecutive RSSI values in dB. By applying the sliding window, the small scale fading is considered to be removed [6]. From D. Vlastaras *et al* [7], we learn that the large scale fading can be modeled as a Gaussian distribution with zero mean and standard deviation. This is verified by observing the residual histogram of the derived large scale fading of measurements. For each LOS and OLOS scenario, one set of parameter is derived and used later in the model to simulate the large scale fading.

Furthermore, the vehicular shadowing is considered spatial correlated and can be more precisely modeled by a correlated Gaussian [15]. The particulars are discussed later in subsection 2.1.7 Correlated Gaussian.

2.1.4 Ordinary Least Squared Estimation

To derive pathloss model from measurements data, an ordinary least squared estimation (OLSE) is typically performed. According to the defined pathloss model, the received RSSI y_i could be modeled as a linear function in dB domain,

$$y_i = \alpha + \beta x_i + u_i, \tag{2.4}$$

where α is the reference value PL_0, β is the pathloss exponential n and u_i represents the large scale fading Ψ_σ which is a Gaussian distribution process in dB domain with zero mean and standard deviation σ [7]. The aim of the OLSE is to minimize the variance of the modeled value against the measurements value which is eventually to minimize the term $s = \sum u_i^2$,

$$s = \sum_{i=1}^{N} u_i^2 = \sum_{i=1}^{N} (y_i - \alpha - \beta x_i)^2, \tag{2.5}$$

To write the model in matrix form, the reference value PL_0 and the pathloss exponent n are combined in a two by one parameter column vector $\hat{\beta} = [PL_0\ n]^T$, where ^{T} is the notation of transpose. The log-distance is also put in a matrix $X = [\mathbf{1}\ 10\log_{10}(\frac{\mathbf{d}}{d_0})]_{L\times 2}$ with L representing observation number of the regarding measurements. $\mathbf{1}$ is a size L column vector of ones, and $\mathbf{d}$ is a size L column vector of the linear distance. Eventually, X is a L by two matrix. The modified pathloss model for the received signal $Y = [PL(\frac{\mathbf{d}}{d_0})]_{L\times 1}$ become, [12]

$$
\begin{aligned}
Y &= X\hat{\beta} + U \\
S &= U'U = u_1^2 + u_2^2 + \cdots + u_N^2 \\
U &= Y - X\hat{\beta},
\end{aligned}
\tag{2.6}
$$

where S is the variance and U is a L by one column vector describing the large scale fading, $'$ is also a notation of transpose. Eventually the equation becomes,

$$
\begin{aligned}
S &= (Y - X\hat{\beta})'(Y - X\hat{\beta}) \\
&= (Y' - \hat{\beta}'X')(Y - X\hat{\beta}) \\
&= Y'Y - Y'X\hat{\beta} - \hat{\beta}'X'Y + \hat{\beta}'X'X\hat{\beta}.
\end{aligned}
\tag{2.7}
$$

To minimize the variance, which is to minimize S, the partial derivation can be calculated on ∂S over $\partial\hat{\beta}$ at S being 0,

$$
\frac{\partial S}{\partial \hat{\beta}} = -2X'Y + 2X'X\hat{\beta} = 0. \tag{2.8}
$$

By solving equation (2.8), the estimation of the parameter $\hat{\beta}$ can be derived,

$$
\hat{\beta} = (X'X)^{-1}X'Y. \tag{2.9}
$$

However, the model only considered the information from received packets, the information of the lost packets should also be included in estimating the practical channel. From the research of C. Gustafson *et al* [12], with a known number of missing data where only the knowledge of the distance is known, it is possible to base the estimation on a censored normal distribution. In this thesis, maximum likelihood estimation (MLE) is employed and explained in the next section.

2.1.5 Maximum Likelihood Estimation

For the measurements at large distances, there is a fair probability that it could be much more missing packets with further sampling. As the data measured is limited by the dynamic range and affected by the noise floor of the measurement systems, the pathloss model calculated from ordinary least squared estimation may lead to a bias estimation from reality. Thus, a maximum likelihood estimation (MLE) is performed here to get a better estimation on the pathloss parameter, which takes censoring situation into consideration.

MLE is a method of estimating the parameters of a statistical model, which is to seek the probability distribution that makes the observations most likely. When applied to a data set and a given statistical model, MLE provides estimates for the model's parameter which maximize the probability of desired term, i.e. the likelihood function.

Given a set of parameter values, the probability density function (PDF) shows that some data can be more probable than others. However, in reality the data set has been already observed and a proper model is also assigned. The demand is to find the desired PDF among all the model prescribed probability densities which have the maximum probability to have produced the given data set. To avoid a complicated multi-dimensional

process and to solve this problem, a likelihood function need to be first determined. It is a function of the parameter which is defined on the parameter scale, given a particular set of observed data. The initial input here could be the previous defined ordinary least squared estimation parameters. In related to that, maximizing the log-likelihood function is often a replacement of maximizing the likelihood function for convenience. Since the logarithm is a monotonically increasing function, the logarithm of a function achieves its maximum value at the same point as the function itself [12]. Eventually, MLE here is to maximize the log-likelihood equation (2.10),

In these measurements, the received packets data are first used to generate ordinary least squared estimation temporal model parameters. Then all the RSSI values below a certain level (i.e. the censoring level) and all the missing data have a probability to be observed based on the distance. The probability of outage packets is generated according to the normal PDF of the chosen censoring level and the temple modeled censored data. The three desired parameters are the pathloss exponent, power reference level and shadowing deviation.

The probability of observing a censored data at distance d is given by [12],

$$P(d_{\text{censored}}) = 1 - \Phi\left(\frac{c - x_i\hat{\beta}}{\sigma}\right), \tag{2.10}$$

where c is the censoring level, which is proper chosen with some margin with respect to the noise floor, so that a limited number of samples dominated by noise are included as measurement data. Φ is the cumulative distribution function (CDF) of the standard Gaussian distribution. The likelihood function can be treated as two parts: likelihood of uncensored data and likelihood of censoring data. This is done by adding an indicator function I_i, and the likelihood function becomes,

$$l(\sigma, \hat{\beta}) = \prod_{i=1}^{N} \left[\frac{1}{\sigma}\phi\left(\frac{y_i - x_i\hat{\beta}}{\sigma}\right)\right]^{I_i} \left[1 - \Phi\left(\frac{c - x_i\hat{\beta}}{\sigma}\right)\right]^{1-I_i}. \tag{2.11}$$

By setting I_i to 1, the likelihood of uncensored data is calculated. For censored data likelihood, I_i is set to 0. To simplify the process, equation (2.11) is transformed to a log-likelihood function. Eventually, the log-likelihood function can be derived and written as,

$$\begin{aligned} L_n(\text{uncensored}) &= \sum_{i=1}^{N} \left[-\ln\sigma + \ln\phi\left(\frac{y_i - x_i\hat{\beta}}{\sigma}\right)\right] \\ L_n(\text{censored}) &= \sum_{i=1}^{N} \ln\left[1 - \Phi\left(\frac{c - x_i\hat{\beta}}{\sigma}\right)\right]. \end{aligned} \tag{2.12}$$

By finding the maximum of the log-likelihood function, the three desired parameters could be found, which would fit best with the given data regarding the censoring.

Generally, MLE become unbiased minimum variance estimators as the sample size increases. One thing to be careful with is that the MLE can be heavily biased if the sample size is small. Also one should be cautious to choose the starting values since the MLE can be very sensitive to that.

2.1.6 Spatial correlation

As mentioned in subsection 2.1.1 channel model, to model V2V as a stochastic time variant system, an auto correlation function is required. Once a vehicle goes into a shadow zone, it remains shadowed for a certain amount of time implying that there is spatial correlation for the vehicular shadowing. The spatial auto correlation function of shadow fading can be written as [5],

$$r_x(\Delta d) = E\{X_\sigma X_\sigma(d+\Delta d)\}. \tag{2.13}$$

where E is the notation of expectation.

As mentioned, V2V shadow fading is not typically a WSSUS process, which, to avoid being entangled with massive complexity, is mostly regarded as an extension of WSSUS. One way to study the characteristic of such channels is to do the experiment repetitively while keeping the conditions the same. That is evidently not feasible in wireless links. The other way is to assume that fading process is an ergodic process. Then one can divide the observations over small regions with the assumption that WSSUS could hold over these regions. In addition to that, the distance dependent mean need to be subtracted from the overall channel gain. After that, the large scale variation of shadow fading can be well described as a Gaussian random variable [5], and the auto correlation function of the Gaussian process can be modeled by an analytical model proposed by Gudmundson [13], which is a simple negative exponential function [3],

$$r_x(\Delta d) = e^{-|\Delta d|/d_c}, \tag{2.14}$$

where Δd is an equally spaced distance vector and d_c is the average decorrelation distance which is a scenario-dependent real value constant. d_c is defined as the value of Δd at which the auto correlation function value is equal to $1/e$.

2.1.7 Correlated Gaussian

In a typical V2V communication, once a link is obstructed by another vehicle, it remains in the shadow for a certain amount of time. The vehicular shadowing is normally modeled as Gaussian distribution with a spatial correlation. For this purpose, a correlated auto regressive Gaussian is employed during the vehicular shadowing modelling.

In order to do that, a normal distributed random sequence g_n is first produced. Then with the correlation model ρ and the correlation coefficient d_c, the correlated Gaussian sequence r_n can be generated as [15],

$$\begin{aligned} g_n &= N(0,1), \quad \rho = e^{-1/d_c} \\ r_n &= \rho^n g_0 + \sqrt{1-\rho^2}\sum_{i=1}^{n} g_i \rho^{n-i}. \end{aligned} \tag{2.15}$$

The correlated Gaussian generation follows with two properties: Each individual generated number is a Gaussian deviate and follows a zero mean unit deviation distribution; auto correlation function of the sequence decays following a certain model with a predetermined decay time. In this case, the model is exponential and decay time is the spatial decorrelation distance according to last subsection.

2.2 Measurements

The measurements took place between Landvetter airport (lat N 57.68014, long E 12.31441) and Borås city (lat N 57.71958, long E 12.96809) at Rv 40 road, Sweden [6]. A normal to rich scattering environment of highway is expected from characterize of the Rv 40 road. Two major measurement scenarios were performed: High-way convoy (Scenario 1a and 1b) and overtaking cars (Scenario 2). The coordinates of several bridges in between the path were used from google map as reference points for time synchronization. The measurements route are shown in Figure 2.1,

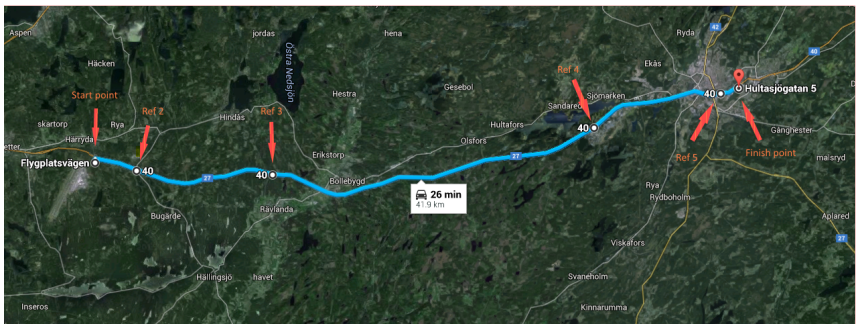

Figure 2.1: The route of the measurements on google map.

Six wireless communication links performance were captured between four Volvo cars of different models (Volvo XC70, S60, XC90 and V70) for each measurement. Each vehicle was equipped with transceivers as receiver and transmitter using IEEE 802.11p communication standard. The transceivers are connected with specially designed vehicular antennas on the roof and transmitted repetitively with a 10 Hz frequency. GPS coordinates were recorded as references to calculate distances between links. Videos together with time stamps were recorded to separate and synchronize LOS/OLOS scenarios, which is manually derived subsequently. OLOS here is defined as the situation where at least one car is in between the RX and TX vehicles constituting the link nodes, which refer to the video as more than half of the vehicle body is blocked by other vehicles visually. This definition is only temporary used in this report, as in many related paper, OLOS could be defined with consideration of the first Fresnel zone.

The measurements results were converted into matlab format with five major subjects for each link: 1, Distances between vehicles; 2, Received RSSI values; 3, Lost packets information; 4, Frame ID; 5, Post time.

As the measurement distances are relatively small based on the ellipsoid model of the earth surface, and the movement area in the measurements can be approximately treated as plane [16]. The distances between two vehicles' GPS points can be calculated by using Pythagorean distance function,

$$Distance = \sqrt{\Delta\Phi^2 \times (\Phi_1 - \Phi_2)^2 + \Delta\lambda^2 \times (\lambda_1 - \lambda_2)^2}, \tag{2.16}$$

where Φ_1 and Φ_2 are the two points' latitude and λ_1 and λ_2 are the two points' longitude. Figure 2.2 shows the definition of the latitude and longitude on an ellipsoid. The normal at a point on the surface of an ellipsoid does not pass through the centre, except for points

on the equator or at the poles. Since the definition of the latitude is the angle between the normal and the equatorial plane, the terminology for latitude must be made more precise by distinguishing. $\Delta\Phi$ and $\Delta\lambda$ are the unit arc length of the ellipsoid that Earth is being modelled. At certain geodetic latitude degree, corresponding values for $\Delta\Phi$ and $\Delta\lambda$ give the value on length for the respectively latitude and longitude.

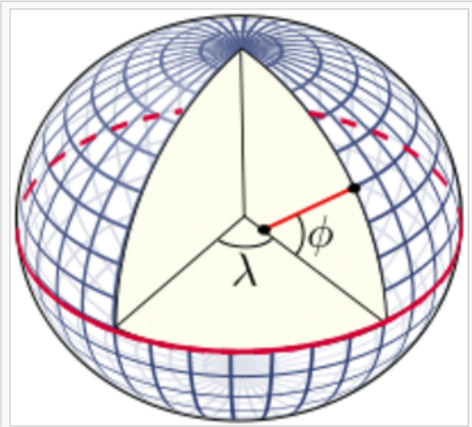

Figure 2.2: The definition of geodetic latitude Φ and longitude λ on an ellipsoid, from [16].

The shape of an ellipsoid is determined by the shape of the ellipse which is rotated about its minor axis. This requires the equatorial radius (a) and the polar radius (b) with the relationship of,

$$\begin{aligned} a &= 6378137m \\ b &= 6356752.3142m \\ e^2 &= \frac{a^2-b^2}{a^2} = 0.00669437999014, \end{aligned} \tag{2.17}$$

where e is the eccentricity. Then based on the evaluation of the meridian distance, for the arc distance on one degree difference latitude and longitude, the $\Delta\Phi$ and $\Delta\lambda$ could be calculated as,

$$\begin{aligned} \Delta\Phi &= \frac{\pi a(1-e^2)}{180(1-e^2\sin^2\Phi)^{\frac{3}{2}}} \\ \Delta\lambda &= \frac{\pi a\cos\Phi}{180(1-e^2\sin^2\Phi)^{\frac{1}{2}}}. \end{aligned} \tag{2.18}$$

As for the data used in this report, the transceivers transmitted packets of size 100 bytes with a 10 Hz repetition rate and the receivers reported RSSI values in the dB domain with 1 dB resolution for successfully decoded packets. As mentioned before, a sliding window with size 10 is used on RSSI values to compensate the hardware limitation of measurements resolution and to remove the small scale fading effect. For the missing packets, as all transceivers were synchronized to GPS, all time stamps without receiving a

packet correctly were recorded. The none reported RSSI values were later assigned with a fairly low values temporally for the relaying simulation (-100 dB in the simulation, as the lowest received RSSI value is about -90 dB). The measurement post time is the time count of Epoch time starting from January 1, 1970 with 0.1 second resolution.

For the relaying simulation, the results of two tri-links were picked from Scenario convoy 1a and 1b, while for each scenario, four vehicles were driving in the same direction as convoy with an average speed of 90 km/h. In scenario 2 overtaking, four tri-links were chosen to be studied. Furthermore, for the statistic model, two censored tri-links data with LOS/OLOS separation were taken into account, while for the joint correlation studies, another four desired cases were picked from scenario convoy. More details are introduced in Chapter 3, 4 and 5 respectively.

In addition to that, data with speed under 30 km/h were removed representing the very beginning and finishing stage of the driving, where the desired highway conditions were not fulfilled. Also the antenna and system loss were manually removed in the RSSI values.

2.3 Relaying scheme

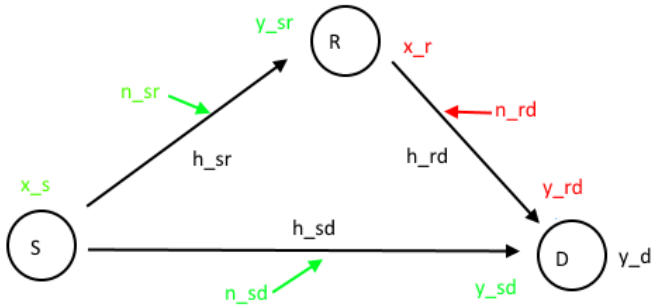

Figure 2.3: A typical single hop relay

Consider a three-node network shown in Figure 2.3. A source transmits information to a destination with the help of a relay. The channels between the nodes are given by h_{sr}, h_{sd}, and h_{rd}. The destination then can use both information from source and relay to make more accurate decision. There are various ways to forward the information through relay. The most common ones are: Amplify-and-Forward (AF), which the relay amplifies the received signal by a certain factor and retransmit it; Decode-and-Forward (DF), which the relay decodes the information and subsequently re-encodes and retransmits it. In another word, is to relay hard decision, parity checking code; another method is Compress-and-Forward which the relay creates a quantized version of obtained signal and forward the regenerated signal to destination [10]. There are also many researches on Hybrid version of the above methods for specify demands. To summarize that, it is a plain comprehension that the relaying provides an extra opportunity for the decoding at the destination, since the transmission could be successful if either independent paths, i.e. source-to-relay-to-destination or source-to-destination, provides sufficient quality [11].

The three nodes, source, relay and destination are displayed in Figure 2.3. The source sends message x_s through channel h_{sr} and h_{sd} which would reach relay and destination respectively. Independent system noise n_{sr} and n_{sd} are introduced separately for both links and the received signals are recorded as y_{sr} and y_{sd} accordingly. At relay, with various relaying scheme operating, the node then prepares new message x_r and send it to destination through channel h_{rd}. Another system noise n_{rd} is added during the process and the received signal from relay is marked as y_{rd}. Finally the combination of the two signals from independent two paths is received at destination. Relations of the signals can be written as,

$$\begin{aligned} y_{sr} &= h_{sr}x_s + n_{sr} \\ y_{rd} &= h_{rd}x_r + n_{rd} \\ y_{sd} &= h_{sd}x_s + n_{sd}. \end{aligned} \tag{2.19}$$

2.3.1 Amplify and Forward

In Amplify-and-Forward, the relay amplifies its received signal, maintaining a fixed average transmit power. The transmit power for the source and the relay is denoted here as P_s and P_r. For general cases in a multi-hop relaying, the power provided by vehicle engines should be equal, $P_s = P_r = P$. The average transmit power for relay is then constrained by a amplify factor β, i.e. $x_r = \beta y_{sr}$ [10].

$$\begin{aligned} &E[(|x_r|)^2] \leq P \\ &\beta \leq \sqrt{\frac{P}{h_{sr}^2 E_s} + 1}. \end{aligned} \tag{2.20}$$

The noise is assumed to be additive white Gaussian noise (AWGN), thus the average noise power is considered to be 1. The receive signal at destination from relay y_{rd} then can be written as,

$$\begin{aligned} y_{rd} &= h_{rd}\beta y_{sr} + n_{rd} \\ &= h_{rd}\beta(h_{sr}x_s + n_{sr}) + n_{rd} \\ &= \beta h_{sr}h_{rd}x_s + h_{rd}\beta n_{sr} + n_{rd}. \end{aligned} \tag{2.21}$$

AF operates at all time, including when SR channel experiences outage. This indicates that the transmission would be most likely failed if the SR-link suffers a depression.

2.3.2 Decode and Forward

Decode-and-Forward is so far the most used one among all the relaying schemes. The relay receives packets from the source and decodes them. If successful, it proceeds and encodes the packets with the same or different encoder as the source's and forwards the packet to the destination. Otherwise, it requests a retransmission from the source or simply stays idle, leaving only the Source-Destination link operating until the next packet arrives. In other words, the signal received by the destination from the delay does not include any additional information about the reliability of the source-relay link. In this

report, the relay uses the same encoder as source if it decodes the signal from source successfully. In that case, the signal forwarded by relay is just the original source signal, $x_r = x_s$.[10]

In this single-hop relay situation, DF always performs better than AF due to the compression of noise at relay. It also opens the possibility for maximizing the coding gain through distributed codes.

2.3.3 V2V Rician channel

Rician fading is a non-deterministic model for the anomaly that occurs when some multipath components of a transmitted signal accidentally cancels one another. It often comes with a LOS component that is much stronger than others. The amplitude gain is characterized by a Rician distribution with Rician factor κ, which indicates the ratio between the power in the direct path and the power in the other scattered paths. With a total power constrain Ω, the relations between the Rician parameters can be written as, [17]

$$\begin{aligned} v^2 &= \frac{\kappa}{1+\kappa^2}\Omega \\ \sigma^2 &= \frac{1}{2(1+\kappa)}\Omega, \end{aligned} \tag{2.22}$$

where v^2 and $2\sigma^2$ represent the power for the two paths, ($\Omega = v^2 + 2\sigma^2$). Furthermore, a Rician distributed number r could be generated accordingly as,

$$\begin{aligned} a &= \sigma \times R + v \\ b &= \sigma \times R \\ r &= \sqrt{a^2 + b^2}, \end{aligned} \tag{2.23}$$

where a and b are the amplitude of the real and imaginary parts respectively, and R is a random number with standard Gaussian distribution.

The V2V radio link can often be modelled statistically as a Rician fading channel. That is a fair assumption with the fact that most V2V links can typically have a LOS component from the direct links with the roof-top antennas. This dominant component in the Rician fading channel is often relatively strong compared to the reflected signal. Thereby, the V2V propagation channel is modelled as a dominant component consisting of a direct LOS wave and a ground reflected wave, a set of early reflected waves and inter-symbol interference caused by excessively delay waves.

2.3.4 MRC at Destination

Under relaying schemes, the destination receiver need to use information both from source and relay. Therefore, a diversity combining has to be performed. Maximum ratio combining (MRC) is implemented which is the optimum strategy to reduce signal fluctuations caused by multipath propagation. The gain of each channel is made proportional to the rms signal level and inversely proportional to the mean square noise level in that channel. The assumptions of the basic condition are restated here: Relay-Destination and Source-Destination are two independent flat fading channels; all the noises are independent and

have standard Gaussian distribution. By that means, the signal to noise ratio (SNR) can be expressed as [11],

$$\gamma = \frac{|h|^2 E_b}{N_0}, \tag{2.24}$$

where γ and h represent the SNR and pre-known channel at relevant link respectively.

With complete channel knowledge, MRC can be performed to improve error rate optimally. As for this measurements, only information on the amplitude of the channel is captured. The MRC used in the simulation is a simplified version which the weights of the combining is only decided by the channel gain.

2.4 Joint correlation

Wireless links under close geographically environment often experience similar large scale fading which could be considered to have correlated fading. Most current multi-link models do not take the correlations between links into account, i.e., cannot accurately represent multi-hop wireless network under certain environment condition. E.g., two links from the same TX would suffer similar loss when the signals pass through or diffract around the same building in its path. In most models, the multi-link would be considered independently, suggesting that if one link suffers fading, the other could still have an independent probability to transmit successfully based on the model parameters, which is not true since both two links are most likely to experience high fading loss. The multi-link correlation would cause a strong limitation on diversity gain in such multipath diversity schemes like ad hoc network.

These multi-link correlations in this report are refer as joint correlation. There are studies on mobile ad hoc networks in Z. Wang *et al* [8] where the implement data are generated from a simulation model and the multi-hop network are considered to be independent and identically distributed random variables (i.i.d.). In P. Agrawal and N. Patwar [9], a random environment measurement was performed with fix position TXs and RXs, the geographical multi-link correlations are analyzed and a statistical model are created. In V2V measurements, TXs and RXs are both with high mobility and yet could still suffer similar environmental shadowing.

In this thesis, a stochastic model is created to simulate the joint shadowing process with consideration of the joint correlation affected by the four dimensional positions of the vehicle and the multi-link vehicles' distance under the same obstruction car.

For a typical ad-hoc network, it is assumed that all nodes have the same configuration and for a single link, the shadowing fluctuation saw from one end is identical to the other. In V2V, the antenna position, vehicle height could differ the channel in some level, but in general, the mutual communication channel can be considered identical. Thereby, the shadowing fluctuations from both TX and RX can be treated the same $s_{TX_i} = s_{RX_i}$ [8].

The shadowing based on the distance $s_{\Delta d_i}$ are modeled as Gaussian with zero mean standard deviation σ_s and the joint correlation R_s based on the movement from TX Δd_T and RX Δd_R are defined in equation (2.25),

$$\begin{aligned} &s_{\Delta d_i}[dB] = N(0, \sigma_s) \\ &R_s(\Delta d_T, \Delta d_R) = E\left\{s_{\Delta d_i} s_{\Delta d_i}\right\}/\sigma_s^2. \end{aligned} \tag{2.25}$$

With the same assumption in Z. Wang *et al* [8], the auto correlations from the TX and the RX are treated independently. This indicates that the joint correlation with both nodes moving is the co-effect of the independently movement with either one of the nodes. With the Gudmundson model [13], the shadowing auto correlation function R_1 and joint correlation function (JCF) R_s are represented below in equation (2.26),

$$\begin{aligned} R_1(\Delta d_R) &= R_s(0,\Delta d_R) = exp\bigg(-\frac{|d_R|}{d_{cor}}\ln 2\bigg) \\ R_s(\Delta d_T,\Delta d_R) &= R_s(\Delta d_T,0)R_s(0,\Delta d_R) = exp\bigg(-\frac{|d_T|+|d_R|}{d_{cor}}\ln 2\bigg). \end{aligned} \tag{2.26}$$

2.5 Sum of sinusoids

The sum of sinusoids (SOS) approach is commonly used to generate Gaussian process. The basic principle is that a stationary Gaussian process can be expressed as a sum of infinite number of sinusoids with random phases and properly selected frequencies [18]. In practice, a finite number N of sinusoids is used to approximate the Gaussian process. A Monte Carlo approach is proposed to randomly generate the sinusoids frequencies in order to simulate WSSUS channels. Since one dimension (1-D) could not completely describe the shadowing effects over a relatively large area (i.e. Cannot capture the spatial correlation when a node moves along a curve rather than straight line), a two-dimensional (2-D) random Gaussian process is introduced. With x and y representing the coordinates of the studied object 2-D movements, the 2-D channel simulation model for the Gaussian process is shown as 2.27 [8],

$$\hat{s}(x,y) \;=\; \sum_{n=1}^{N} c_n \cos(2\pi f_{x,n}x + 2\pi f_{y,n}y + \theta_n), \tag{2.27}$$

where $\{\theta_n\}_{n=1}^{N}$ are random variables uniformly distributed over $[0,2\pi)$. f_x and f_y are two spatial frequencies randomly generated according to specific PDF to sample the 2-D power spectral density of the desired Gaussian random process. In this way, the model is able to have a 2-D auto correlation function to describe the 2-D spatial correlation. $\{c_n\}_{n=1}^{N}$ is the constants obtained from the shadowing process power spectral density. The number of sinusoids N should be relatively large to approximate the 2-D power spectral density more accurately.

In order to generate above parameters, the auto correlation function and power spectral density of the shadowing process need to be derived. As mentioned in equation (2.13) and (2.14), an exponential auto correlation function which could fit this measurements data is given by 2.28,

$$R_s(\Delta x,\Delta y) = R_s(d) = e^{-ad}, \tag{2.28}$$

where $a = \ln 2/d_{cor}$ is a constant depending on the environment with the decorrelation distance d_{cor} calculated, and $d = \sqrt{\Delta x^2 + \Delta y^2}$ is the distance of the node's movement. To obtain the 2-D power spectral density, a 2-D Fourier transform is performed on the auto correlation function $R_s(\Delta x,\Delta y)$ which gives rise to equation (2.29),

$$\begin{aligned}\Phi_s(\Delta x,\Delta y) &= \int_{-\infty}^{\infty}\int_{-\infty}^{\infty} e^{-a\sqrt{x^2+y^2}} e^{-j(2\pi f_x x+2\pi f_y y)} dxdy \\ \Phi_s(f_r) &= \frac{2\pi a}{\left[a^2+4\pi^2 f_r^2\right]^{\frac{3}{2}}},\end{aligned} \tag{2.29}$$

where f_r is defined such that $f_x = f_r cos(\varphi)$ and $f_y = f_r sin(\varphi)$. From studies in [18], the sampling frequencies can be generated according to a PDF which is proportional to the power spectral density of shadowing. The joint PDF in the 2-D model can be expressed as $p(f_x,f_y) = b\,\Phi_s(f_x,f_y),\ f_x > 0$. b is 2 here as a constant to normalized the PDF. Following the procedure, the PDF $p(f_r,\varphi)$ and CDF $P(f_r)$ of the random spatial frequencies could be derived as equation (2.30),

$$\begin{aligned}p(f_r,\varphi) &= \frac{2\pi ab}{\left[a^2+4\pi^2 f_r^2\right]^{\frac{3}{2}}} \\ P(f_r) &= 1-\frac{a}{\sqrt{a^2+4\pi^2 f_r^2}}.\end{aligned} \tag{2.30}$$

Inverse the CDF function, the random variable f_r then can be generated based on a uniformly distributed random variable β over $\left[0,1\right)$ and the 2-D spatial frequencies can be derived as equation (2.31),

$$\begin{aligned}|f_r| &= \frac{\alpha}{2\pi}\sqrt{\frac{1}{(1-\beta)^2}}-1 \\ f_x &= |f_r|\cos(\varphi),\ f_y = |f_r|\sin(\varphi) \\ \theta_n &= U(0,2\pi),\end{aligned} \tag{2.31}$$

where φ and θ are two uniformly distributed random variables over $\left[0,2\pi\right)$. The 2-D spatial frequencies could be generated corresponding to equation (2.27), the power coefficient $\left\{c_n\right\}$ have the same value for all sinusoids in order to keep the process stationary. The value is defined by the total power of the Gaussian process and for unit power it can be expressed as $c_n = \sqrt{\frac{2}{N}}$.

As mentioned in previous section, the joint correlation of shadowing at TX and RX is assumed to be independent processes. As a result from [8], the auto correlation function and power spectral density for the joint shadowing have the same form as single link, considering equation (2.26). Also the PDF and CDF of the random spatial frequencies for TX and RX are identical. Based on the same principle above, the 2-D sum of sinusoids can be extended to a 4-dimensional (4-D) sum of sinusoids function,

$$\hat{s}(x,y,u,v) = \sum_{n=1}^{N} c_n \cos(2\pi f_{x,n}x+2\pi f_{y,n}y+2\pi f_{u,n}u+2\pi f_{v,n}v+\theta_n), \tag{2.32}$$

where (x,y) and (u,v) represent the positions of TX and RX respectively. $f_{u,n},\ f_{v,n}$ are 2-D spatial frequencies for RX and are generated independently but in the same way as $f_{x,n},\ f_{y,n}$ from equation (2.31).

Under the same concept, in this thesis it is assumed that the auto correlation of the vehicular shadowing affected by the vehicle distance under the same obstruction is independent from the auto correlation for the vehicles' movements. By modeling the auto correlation of the shadowing affected by distance, it is possible to add the correlation properties to the sum of sinusoids stochastic model.

Chapter 3
Relaying Performance

In order to study the relaying performance on V2V systems, a bit-level simulation is employed. Every measured RSSI value represents the average channel power at a certain observation period, and it is used as the mean power of the simulated Rician channel. Random packets are generated and sent through the simulated channels based on different relaying schemes. Individual results of packet error rate (PER) are recorded.

3.1 Simulation set up

3.1.1 Packet generation

The sizes of the packets in the measurements are 100, 500 and 1500 bytes per packet and the corresponding RSSI results are recorded individually. In this thesis, only RSSI results of packet size 100 are used. Therefore, all the random generated packets for the simulation are in the same size. An example of packet generation is demonstrated in Figure 3.1,

Figure 3.1: Packet generation

The packets are generated from random binary bits. After a proper number of bits are generated, a cyclic redundancy check (CRC) is implemented and used later in the receiver to check whether the original information is decoded correctly. Then a general coding is utilized to enhance the transmission quality. For this thesis, Viterbi Algorithm (VA) is chosen and a regular convolutional coding with trellis 6, $[77\ 45]$ is employed. The encoding rate is $1/2$. Eventually, QPSK modulation is performed and packets with size 100 are ready to be sent. [11]

3.1.2 Channel and Power factor

All channels used in the simulation are modified based on the RSSI values recorded by each vehicle. Each RSSI value for one specific observation gives information of the mean receive signal power for the entire packet. As mentioned in Chapter 2.3, in order to be

more accurate on the bit-level simulation, for every packet passing a particular observation, all bytes of the packet are considered to pass through a Rician distribution channel individually with a mean power of the corresponding RSSI value. Each sub-channel introduces independent noise. The Rician factor κ is chosen to be 3 in this simulation as a general choice for V2V channels [19].

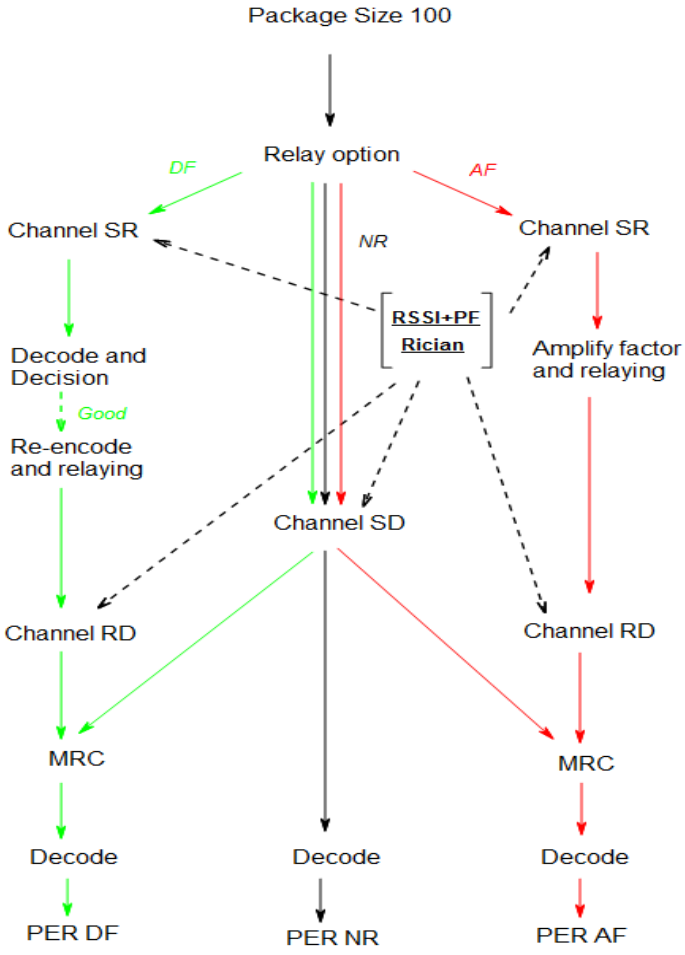

Figure 3.2: System block for relaying simulation

A power factor (PF) is introduced to determine the simulated transmit power and to revise the level of packet error rates within the interested region. The initial value of PF is determined when the packet lost rate (PLR) of the non-relaying case to be around 20%. The PLR here is defined as the ratio between total number of lost packets and total number of sent packets.

Together with the two relaying schemes, Decode-and-Forward (DF) and Amplify-and-Forward (AF) discussed in chapter 2.3, the system block is demonstrated in Figure 3.2,

For each observation, one hundred generated packets are sent from the source. Each

of the packets reaches the relay, that react based on the individual schemes, i.e. DF, AF or non-relaying (NR). Firstly, the signal symbols in all three schemes reach the destination through the source-destination (SD) channel, regardless of any action token at the relay. The destination receives the signal symbol and either uses it as one of the two spatial diversity compositions in the maximum ratio combining, or directly passes it to the destination decoder as a solo component in the non-relaying case. Secondly, in the two relaying schemes, the relay also receives the signal from the source. Since the propagation distance of the source-relay (SR) link is normally shorter than the SD, also the SR channel has a proper chance not being blocked by an obstruction when SD is, the power of SR channel is expected to be higher than the SD channel in general. In DF scheme, the relay decodes the received symbol and makes a hard decision according to the cyclic redundancy check results. If the result indicates a fail transmission on the SR link, the relay remains idle until the next packet arrives. Otherwise, the successfully decoded signal is re-encoded with the same encoder as source's and is forwarded to the destination with an unit power. In the end, at the destination, the two received signals, one being the re-encoded symbol passed through RD channel, the other being the signal comes directly from the source through SD channel, are combined with maximum ratio combining (MRC). The combined signal is decoded and after sending all hundred packets for this specific observation, a packet error rate is calculated. As for the AF, the simulation scene is mostly the same with the DF, except that at the relay, there is no decode of the received symbol, instead the relay amplified whatever it receives by a calculated amplify factor according to equation (2.20) and forward it to the destination. Finally, for all three schemes, this entire process happens for every measured observations from the chosen continuous period and the PER results can be compared between different relaying schemes.

3.2 Scenario convoy

3.2.1 Scenario Initial

As previously mentioned in Chapter 2.2, for each typical measured four-car links, three of the cars are picked as study subjects.

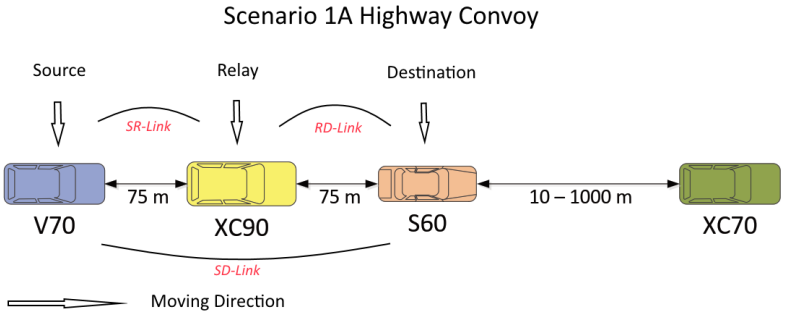

Figure 3.3: Test scenario 1a. Distances are not correctly scaled.

As Figure 3.3 illustrated, the V2V links V70-XC90-S60 are picked and representing

Scenario 1a in the relaying simulation. The received RSSI values measured on vehicle XC90 from V70 are considered as the channel gain of the source-relay (SR) link, and similarly the received RSSI values measured on vehicle S60 from V70 and XC90 are considered as the channel gain on the source-destination (SD) link and the relay-destination (RD) link respectively. The interrelated links from TX to RX and RX to TX are assumed to be identical. In these chosen links, the variations of the distances between vehicles are generally small. The maximum variation value is less than 100 meter.

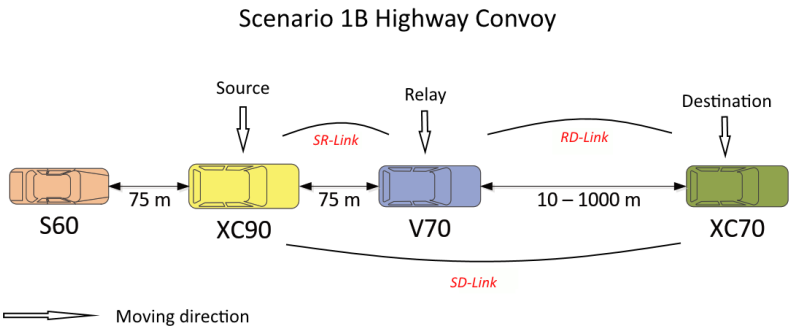

Figure 3.4: Test scenario 1b. Distances are not correctly scaled.

As Figure 3.4 demonstrates, the V2V links XC90-V70-XC70 are picked and representing Scenario 1b in the relaying simulation. The received RSSI values measured on vehicle V70 from XC90 are considered as the channel gain of the SR link; and similarly the received RSSI values measured on vehicle XC70 from XC90 and V70 are considered as the channel gain of SD link and RD link respectively. In these chosen links, vehicle XC70 regularly changes its distances from the other two vehicles. As a result, data with a higher range of vehicles' distances can be observed.

For each simulation, the implemented RSSI values are measured from an continuous time period with approximately 12000 observations (20 minutes).

3.2.2 Relaying Results

The results of relaying simulation with Non-relaying (NR), Decode-and-Forward (DF) and Amplify-and-Forward (AF) schemes for scenario convoy are presented and discussed in this subsection.

Firstly, multiple power factors are tested with NR scheme in order to adjust an appropriate reference level based on the packet lost rate which are introduced in 3.1.2 channel and power factor subsection. As a result, the selected power factor for the basic simulation is 3×10^7, which is 74.77 in dB. The corresponding packet lost rate for the NR is around 18.15% and the packet error rate results for the NR, DF and AF are displayed separately in Figure 3.5, Figure 3.6 and Figure 3.7,

As can be seen from Figure 3.5, Figure 3.6 and Figure 3.7, the X axis shows the simulated continuous observation period, the Y axis shows the number of the failure decoded packet at the destination for each observation, and as a reminder, 100 packets are sent for each observation in the simulation. It is evident that the packet error rate performances

for the transmission with DF and AF relaying schemes outperform NR. The packet lost rates (PLR) are compressed by relaying from around 20% down to a level within 10%. With DF scheme, the PLR number is even pushed to around 5%. Apart from the exceptional bad behaviors around observation number 3500, 6000 and 11000 which is deduced to be a rapidly increase in distance from 50 to over 250 meter, the relaying graphs (DF as green, AF as blue) clearly suggest that there is a significant benefit of implementing relaying schemes to V2V systems. The measured channels for the three chosen links are plotted in Figure 3.8 to evaluate the observation periods with high packet error rate. All the RSSI values of missing packets are represented with -100 dBm. In general the SR link (Blue) is under a superior condition while the SD link (Red) is under a substandard one

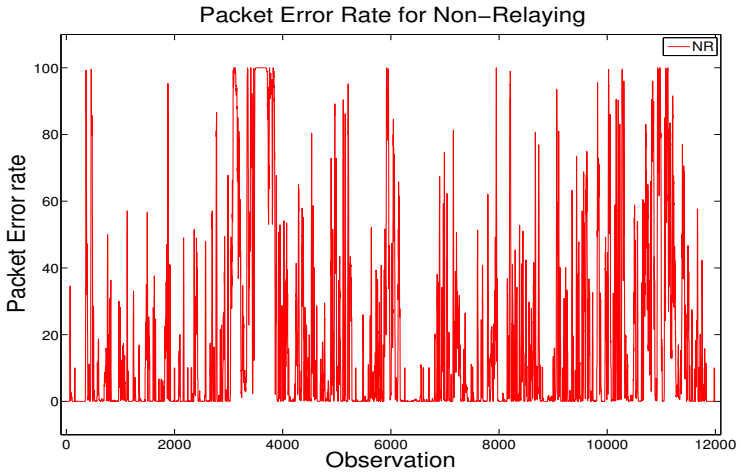

Figure 3.5: PER results NR, PF 3e7, Scenario 1a

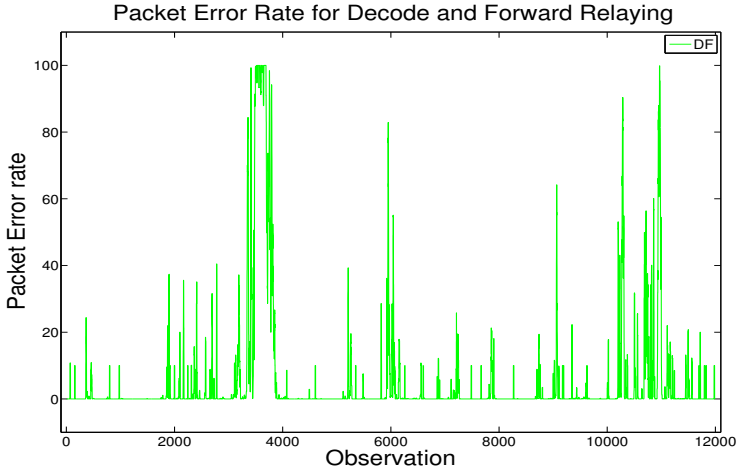

Figure 3.6: PER results DF, PF 3e7, Scenario 1a

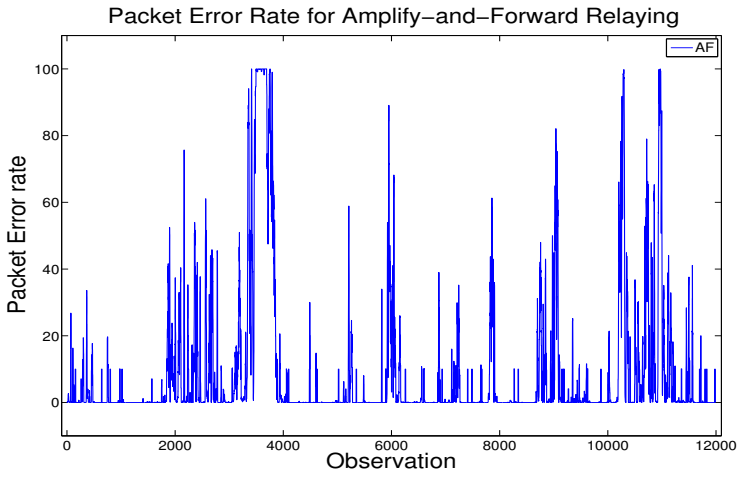

Figure 3.7: PER results AF, PF 3e7, Scenario 1a

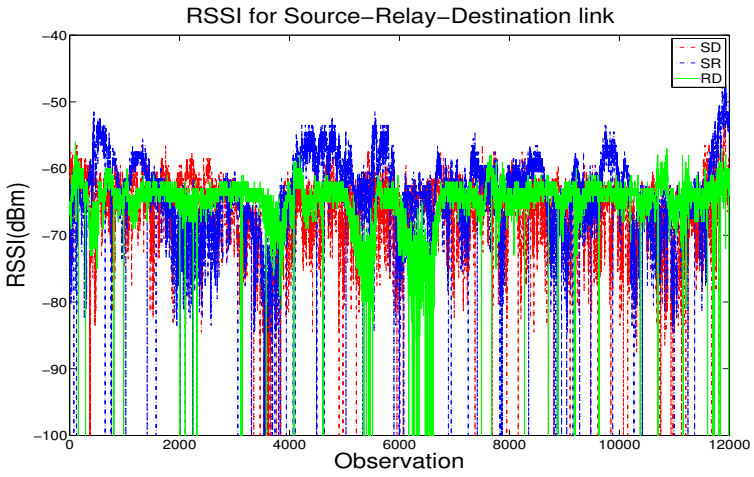

Figure 3.8: Measured RSSI for relaying links, Scenario 1a

as expected. The corresponding packet error rate results generally rise and fall with the RSSI values being low and high.

As a continuation, the power factor are gradually increased to see the degree of improvement of the packet lose rate regarding the three relaying schemes. Tested values are 3×10^7, 4.5×10^7, 6×10^7, 7.5×10^7 and 9×10^7 in linear domain. All the numerical results are listed in Table 3.1 and the simulation results for comparison of NR and DF are illustrated in Figure 3.9.

The improvement rate of the packet lost rate gradually decreases as the power factor further increases. After certain level, the influence on the packet lost rate of increasing the power factor is relatively insignificant, e.g., when the power factor increases from $7.5 \times$

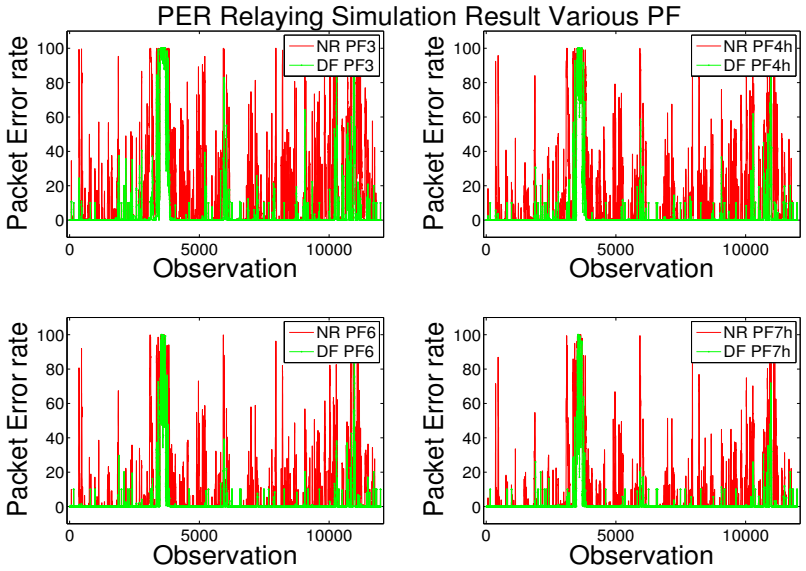

Figure 3.9: PER simulation results, various PF, Scenario 1a

PLR Numerical Result for Convoy			
Scenario and PF	NR	DF	AF
Convoy 1a, 3e7	18.15%	5.49%	9.07%
Convoy 1a, 4.5e7	13.07%	3.64%	6.18%
Convoy 1a, 6e7	10.21%	2.77%	4.86%
Convoy 1a, 7.5e7	8.39%	2.24%	4.04%
Convoy 1a, 9e7	7.12%	1.85%	3.47%

Table 3.1: PLR numerical result for convoy

10^7 to 9×10^7, the increment results of packet lost rate for the NR, DF and AF schemes are only 1.27%, 0.39% and 0.57% respectively. Nevertheless there are still significant improvements with comparison of the two relaying schemes to the NR, e.g., the packet lost rate still has a increment of 5.27% comparing the DF to the NR with the power factor being the highest tested value 9×10^7.

As for Figure 3.9, the red line represents the packet error rate results of the NR, while the results of the DF are represented by the green line. The results of power factor being 9×10^7 are not shown in the figure since only a negligible degree of accumulation is denoted on the transmission performance.

The packet error rate results of the two relaying schemes, the DF and the AF indicate that the DF relaying scheme always outperforms the AF in this simulation. This is because that with the way of implementation in the simulation, the DF unilaterally compresses noise at the relay while the AF amplifies it. If the SR link is under good condition, both the DF and the AF could perform well with a limited effect by noise. However if the

SR link is bad, the DF could recognize the situation and response via various methods, which in this case, it eliminates the bad SR channel effect by remaining idle, while the AF would only enlarge the negative effect by amplifying the noise which more likely leads to an transmission error at the destination. The cumulative density functions (CDF) of the packet error rate for the NR, the DF and the AF with various power factors are shown in Figure 3.10 to further verify the summary.

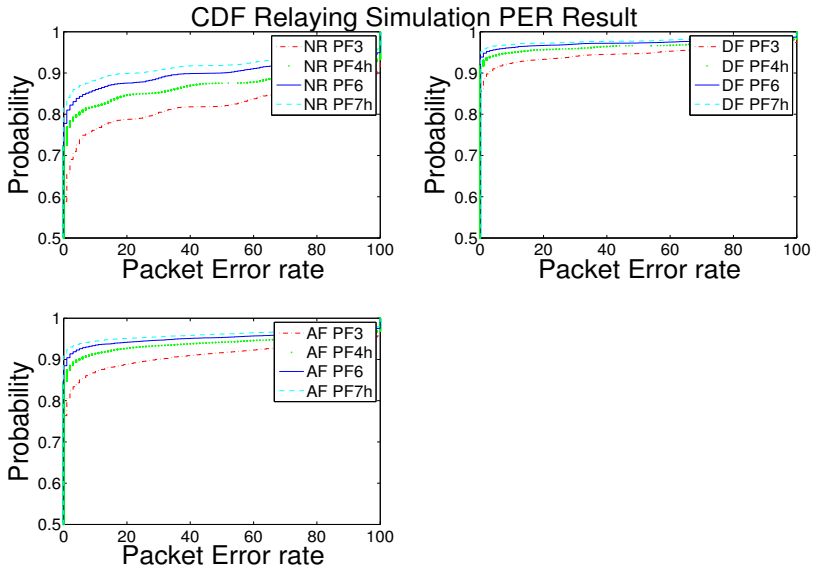

Figure 3.10: CDF simulation results, various PF, Scenario 1a

As can be seen in Figure 3.10, the results of the four power factors in an ascendant order correspond to the color in red, green, blue and cyan. The probability is displayed from 0.5 to 1.

To summarize, the relaying simulation results indicate that implementation of the multihop technology in V2V systems could conspicuously increase the performance of communication as to overcome the issue with shadowing caused by other cars.

3.3 Scenario 2 overtaking

Several more relaying simulations are implemented on overtaking scenario. Four tri-links from the measurements of scenario 2 are picked: Link 1, S60-V70-XC70, which the vehicle queueing sequence changes the least during the entire overtaking process; Link 2, S60-V70-XC90, which the vehicle queueing sequence changes the most; Link 3, S60-XC90-XC70 and Link 4, V70-XC90-XC70, have a moderate changes. The four links are demonstrated in Figure 3.11.

As the Figure 3.11 shows, for the entire duration of overtaking scenario, the XC90 first moved to the last position of the queue, then the V70 changes its lane and accelerates for a certain amount of time. After that, the V70 slowly decreases the speed while the

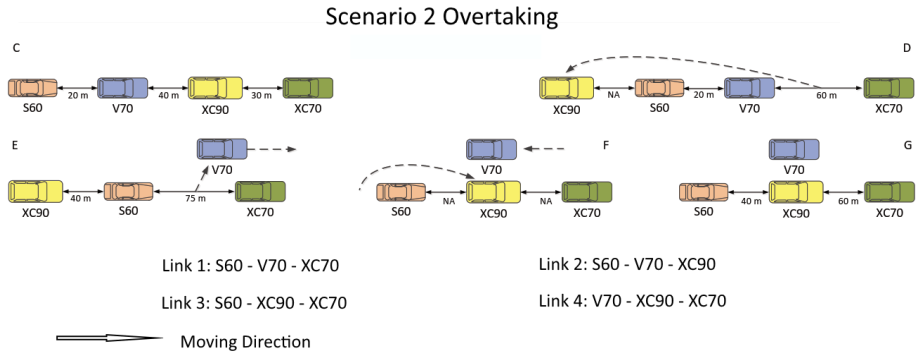

Figure 3.11: Test scenario 2 Overtaking

XC90 moves back to the second position of the queue. Eventually the V70 and the XC90 are steady at the second position of the queue in parallel.

The numerical results for the overtaking scenario are listed in Table 3.2.

PLR Numerical Result for Overtaking			
Scenario and PF	NR	DF	AF
Overtaking Link 1, 6e7	26.91%	3.99%	4.19%
Overtaking Link 2, 4.5e7	24.93%	1.28%	1.48%
Overtaking Link 3, 7.5e7	24.11%	9.78%	16.83%
Overtaking Link 4, 1.5e7	25.66%	12.09%	16.76%

Table 3.2: PLR numerical result for overtaking

During these simulations, four different power factors are employed to preserve the packet lost rate level of the non-relaying to be around 20%. Therefore, it is not distinct to straightly compare the results between the four links. However it is still perceptible that the transmission performance can benefit from the relaying significantly, e.g., in the link 2, the Decode-and-Forward and Amplify-and-Forward compress the packet lost rate from around 25% to around 1%. On the other hand, there are situations with a slighter improvement like the link 3 and link 4, where the packet lost rates only decrease to a level between 10 to 15%. These behaviors of the relaying in overtaking scenario require further understanding based on the detail environment.

In order to compare the scenarios of the chosen links, the simulation packet error rate results and the RSSI data are plotted in Figure 3.12.

The four studied links have various channel conditions which can be seem from the RSSI vs Observation plots in each last sub-figures. The green line represents the relay-destination (RD) link, the blue one represents the source-relay (SR) link and the red line represents the source-destination (SD) link. The blue line is the lowest curve most of the time since the general vehicle distances of the SD link are larger than the other two links. As discussed before, for the link 1 and the link 2, the relaying performances are outstanding which reduce the packet lost rate from around 25% to a level below 5%. For

the link 3 and the link 4, the relaying performances are less remarkable compared to link 1 and link 2, yet they still have a decent reduction on the packet lost rate.

One thing to specify is that, for the link 3, the power factor is set to $7.5x10^7$ which is the highest among all four links. However the packet lost rate result of Amplify-and-

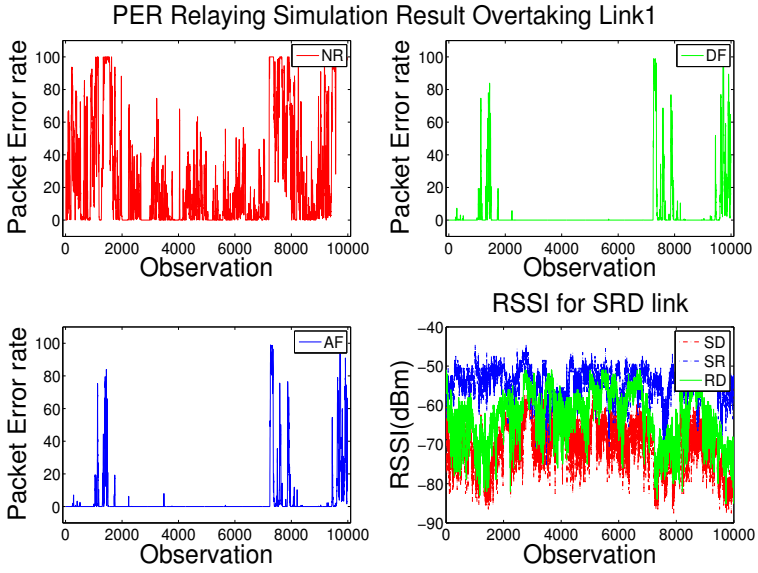

(a) PER result, PF 6e7, scenario 2, link 1

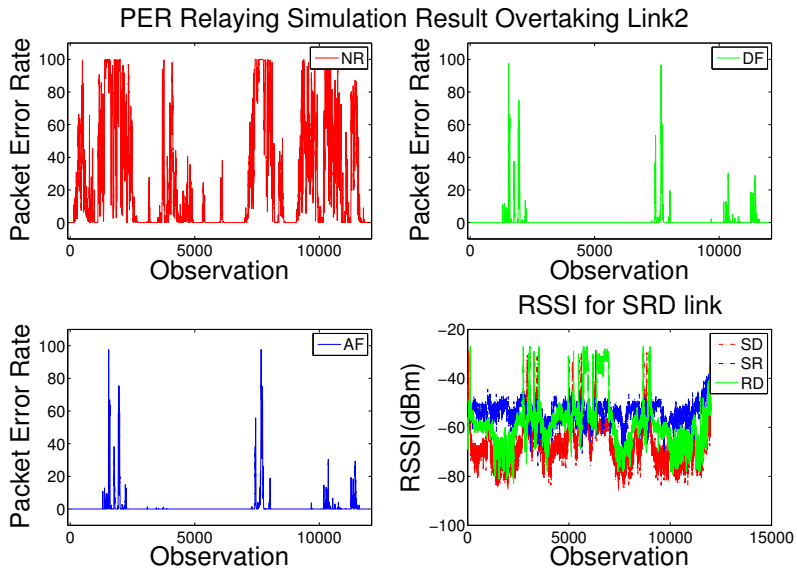

(b) PER result, PF 4.5e7, scenario 2, link 2

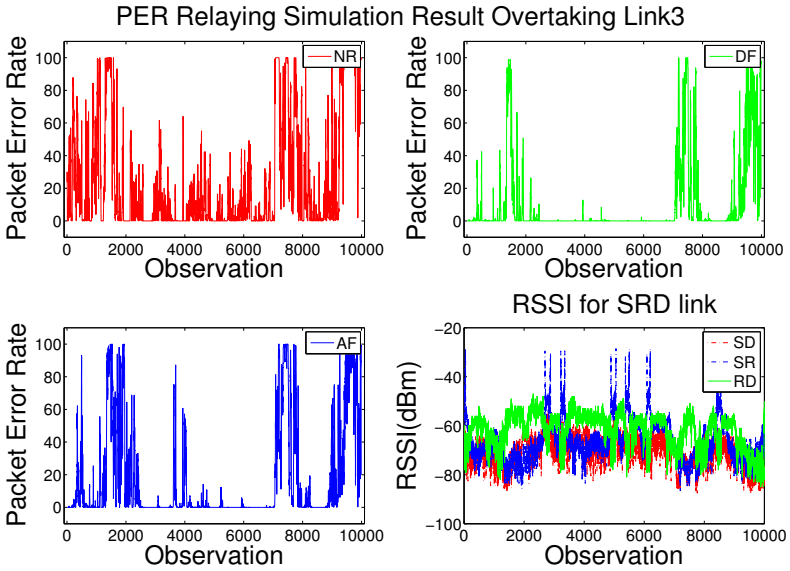

(c) PER result, PF 7.5e7, scenario 2, link 3

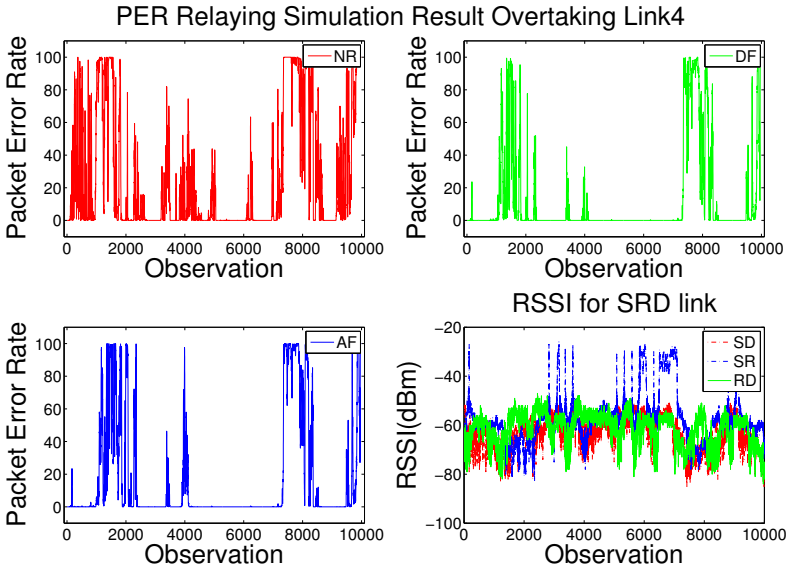

(d) PER result, PF 1.5e7, scenario 2, link 4

Figure 3.12: PER results for scenario overtaking

Forward (AF) is about 17% which is really a poor performance considering the result of Non-relaying 24% and the related results of the other three links. To countercheck

the results, the packet lost rate for the SR link in the link 3 has a high value of 15%. This relatively bad behavior of the SR link could be the essential reason for the poor AF performance and it could be influenced by the antenna positions on the vehicles. The relay vehicle which is the tall XC90 has its antenna on the back of the roof. When the XC90 is overtaking and drops back to the last position of the convoy queue, the relay antenna could be blocked by the tall vehicle XC90 itself which ultimately changes the propagation environment and results to a relatively bad SR channel. This could be inspected from the last subfigure of figure 3.12 (c), where the RSSI values for the SR link (blue line) remain low for most of the time for the link 3, while it is generally the highest among all the other three links.

Chapter 4

Statistic Pathloss and Shadowing Model

In this chapter, the statistics of the pathloss exponent, reference power of the pathloss model based on maximum likelihood estimation are derived from the two chosen tri-link from scenario 1a and scenario 1b. The distribution of the large scale fading is verified in a residual plot and the deviation of the large scale fading is calculated. Then the spatial correlation coefficient of the derived large scale fading is obtained. It is later used to simulate the vehicular shadowing for the measured channel based on the correlated Gaussian approach. The modeled channels are evaluated with the comparison of the measured channels. Finally, a pattern of the packet error rate results versus the channel power is created based on the results of the multiple simulations with various power factors. It is used to directly estimate the packet error rate performance for the simulated channels.

4.1 Pathloss model LOS and OLOS

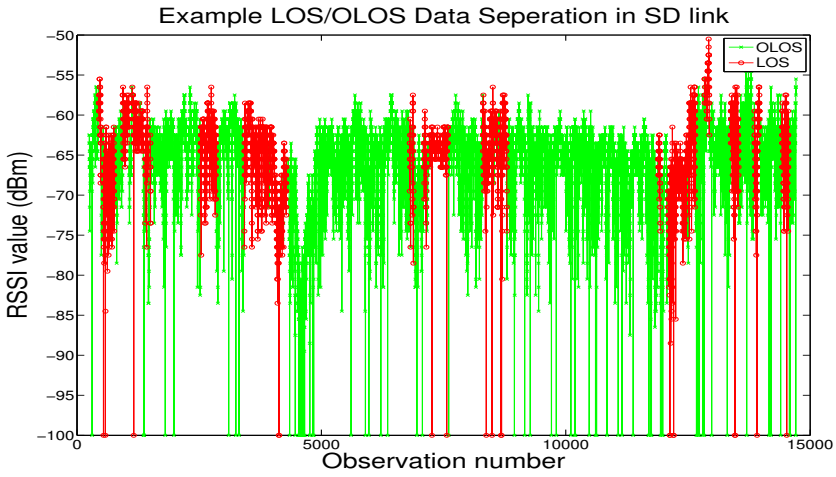

Figure 4.1: Example LOS/OLOS RSSI separation SD link

In order to study the characteristics of the line-of-sight (LOS) and the obstructed LOS (OLOS) scenarios separately, the measured data of the two scenarios are manually synchronized and detached based on the inspection of the on-board videos. An example of data separation for a source-destination (SD) link is demonstrated in Figure 4.1. The LOS data is represented by red and the OLOS data is represented by green. All RSSI values of missing packets are indicated by -100 dBm.

To increase the accuracy of the channel model, all available data from both measurements of scenario convoy is evaluated. Based on the single slope pathloss model in equation (2.1) and the implementation of maximum likelihood estimation discussed in Chapter 2, two linear regression lines are drawn on the RSSI scatter plot vs the distance in dB domain, the green one is the ordinary lease squared estimation (OLSE) and the red one is the maximum likelihood estimation (MLE). The plot is shown in Figure 4.2.

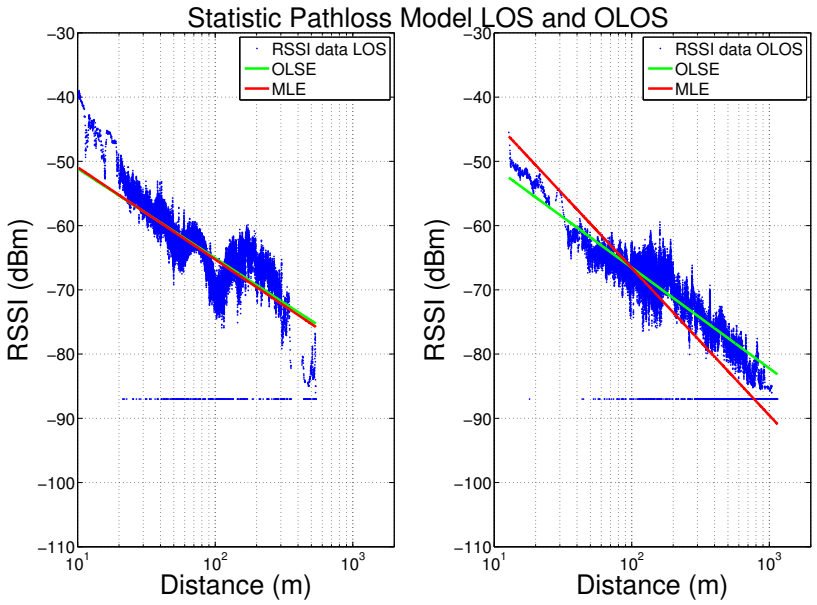

Figure 4.2: Scenario convoy LOS/OLOS pathloss model, OLSE and MLE

The plotted data is filtered with a sliding window of size 10. From the two figures above it can be observed that, the maximum likelihood estimation always has a higher slope than the ordinary least squared estimation curve since the maximum likelihood estimation takes the censored data into consideration. The censoring happens with all the values that are of missing packets or having a receive power lower than a chosen censoring level. These values are considered not clearly received (i.e. being censored) and have a certain probability of successful reception. In this thesis, the censoring level is chosen to be -87 dBm which better describes the information of the missing packets based on the RSSI and distance values. In Figure 4.2, all the data under censoring is plotted as -87 dBm for inspection. In the OLOS scenario, the maximum likelihood estimation curve is much sharper than the ordinary least squared estimation curve while there is only slightly

distinction in the LOS scenario. This is because most censoring happens in the OLOS scenario since the signal is obstructed and there are a lot of measurements happened at large distances between the vehicles.

Furthermore, in the RSSI data of the LOS scenario, there is a clear multi-ray behavior which is caused by the additive and subtractive combination between the dominant LOS component and the reflective ground wave component. In addition to that, since the component of reflective wave always weaken the other after a certain distance, a dual-slope pathloss in the LOS scenario can be observed separated from distance around 180 meter. These behaviours can be further modeled as discussed in C. Sommer *et al* [20] and Chapter 2.1.2. These models are not implemented in this thesis. The multi-ray and dual-slope behaviours are not seen in the OLOS scenarios, since both the two wave components are likely blocked by the obstructed vehicle.

Pathloss model results			
Scenario	Exponent	Reference power	LSF deviation
LOS	1.43	50.9	4.59
OLOS	2.29	43.6	5.82
Overall	2.02	46.3	5.19

Table 4.1: Pathloss model parameters

The final pathloss results for the LOS, OLOS and overall scenarios are illustrated in table 4.1, where the reference power is the power loss at distance of 10 meter,

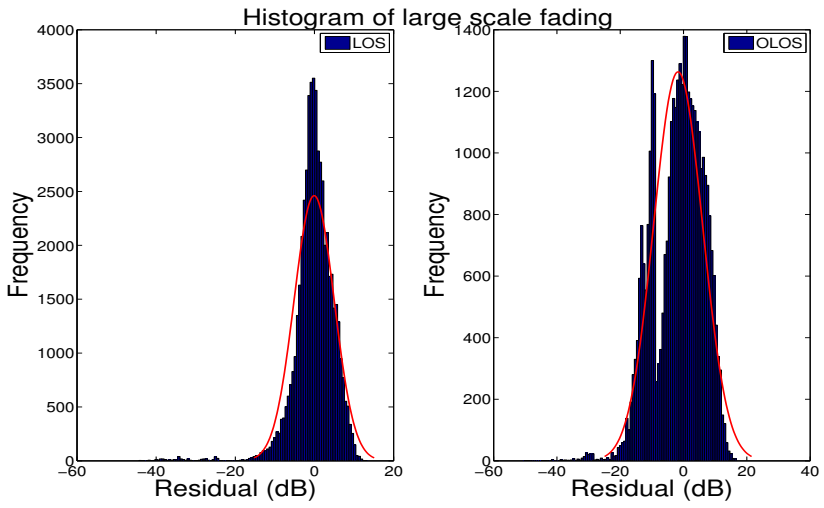

Figure 4.3: LSF residual histogram for LOS and OLOS

To verify the shadowing power distribution, the large scale fading is derived for the LOS and OLOS scenarios individually by subtracting the distance dependent power mean from the measurement RSSI values. The histograms of the residual values are shown in Figure 4.3,

As can be seen from the figure, the derived large scale fading follows a zero mean Gaussian distribution. One thing to mention is that, in the OLOS scenario, the distribution shape of the residual has some distinction with a Gaussian. This is because the pathloss model used for the large scale fading derivation is based on the maximum likelihood estimation, and as discussed before, the OLOS scenario is further affected by the maximum likelihood estimation. As to the offset in the histogram of OLOS, the censored data is taken into consideration during the derivation of the large scale fading, while the histogram only shows the residual values of the uncensored data.

4.2 Spatial correlation

The auto correlation function (ACF) of the shadowing is calculated based on equation (2.13). The LOS and OLOS scenarios are separated to find the correlation coefficient for individual situation. An example of ACF calculation is illustrated in Figure 4.4 for 500 continuous large scale fading data (50 seconds).

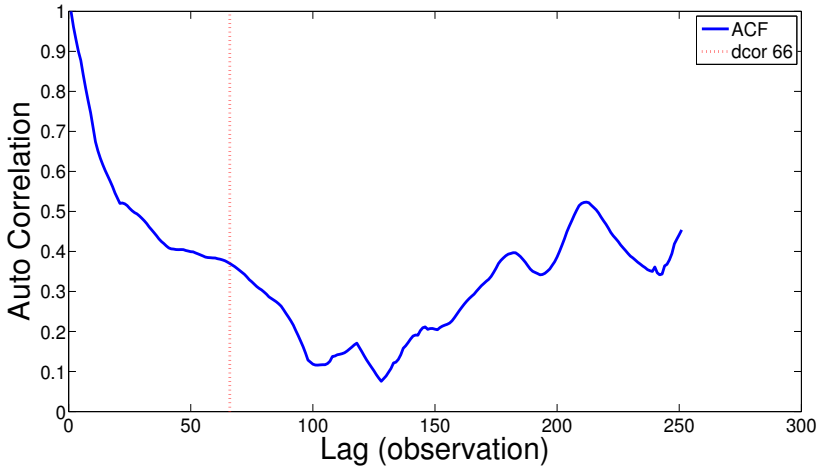

Figure 4.4: Example of ACF for 500 continuous LSF data

In Figure 4.4, each point represents the correlation of all observation pairs with a certain lag. E.g, the value at lag 50 indicates correlation for all data pairs that have a space of 50 observations. As in the equation (2.14), the desired correlation coefficient is the lag when correlation drop from 1 to $1/e$ which in this case is observation number 66. The correlation coefficients of every 500 continuous data are calculated regarding the LOS and OLOS scenarios. An example of the decorrelation distance calculation in one continuous time period is shown in Figure 4.5.

The X axis in this figure is a continuous LOS scenario from source-relay link with around 11500 data observations. For every continuous 500 data points starting from certain observation, a decorrelation distance is calculated and plotted in the graph. The green cross points represent the decorrelation distances calculated at certain start observation, while the red points represent those with the correlation coefficient higher than 500.

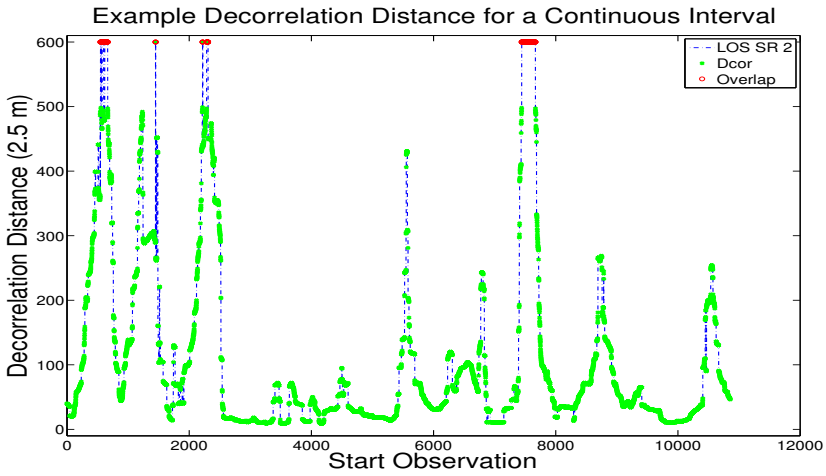

Figure 4.5: Example correlation for a continuous time period

From Figure 4.5, it can be seen that, the decorrelation distance appears to be quite sensitive to the environment. Under certain conditions, it could remain small around 20 to 50 observations indicating a less correlated situation, while occasionally it could raise rapidly over several hundred within a few tens of seconds indicating a high correlation event. The spacing between observations have a time period of 0.1 second. Under an average speed of 25 m/s, the average decorrelation distance for LOS scenario is calculated to be 375 meter (150 observations) and for OLOS to be 500 meter (200 observations).

4.3 Simulation with a statistical model

With the deviation of the large scale fading and the spatial correlation coefficient, a correlated Gaussian shadowing process could be simulated. The simulation of the channels would be simply adding the generated shadowing onto the distance dependent mean pathloss based on the pathloss model regarding LOS and OLOS. The shadowing for different observations with the same distance are generated independently. The spatial correlation coefficient used in LOS is $d_{cor} = 150$ observations and in OLOS is $d_{cor} = 200$. They are derived from the auto correlation function of the large scale fading which is discussed in the previous section. To simulate the channels, all channel observations are simulated based on the LOS and OLOS scenario, employing the corresponding pathloss shadowing model. An example of simulated channel for source-relay link is illustrated in Figure 4.6.

In Figure 4.6, all the values are compensated with the power factor of $3x10^7$ (74.77 dB). The red curve is the mean pathloss following the changes of distance between cars. The modeled channel is demonstrated in cyan and the measured channel is shown in blue. As can be seen, the simulated channel could closely describe the characteristics of the measured channel.

To further evaluate the model, all the channels used in simulation scenario con-

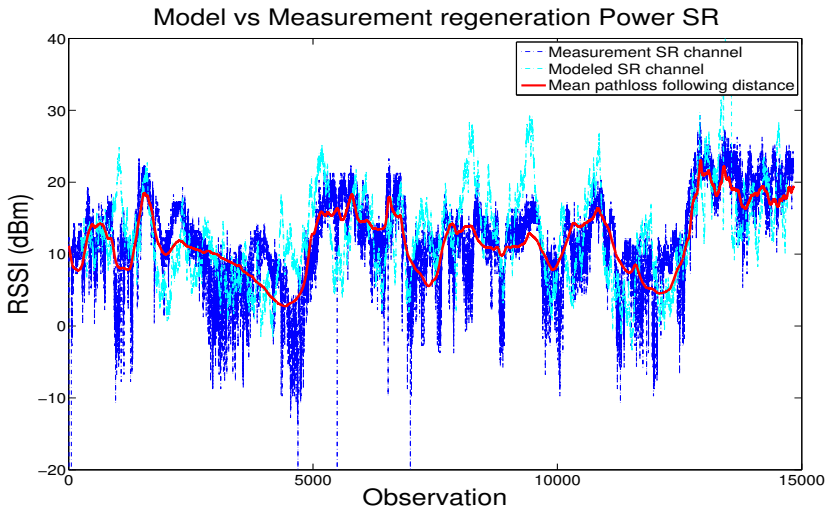

Figure 4.6: Example simulated vs measurements SR channel

voy 1a are simulated, the source-relay (SR), the relay-destination (RD) and the source-destination (SD), based on the vehicle distances and LOS/OLOS scenarios. The power simulations are illustrated in Figure 4.7,

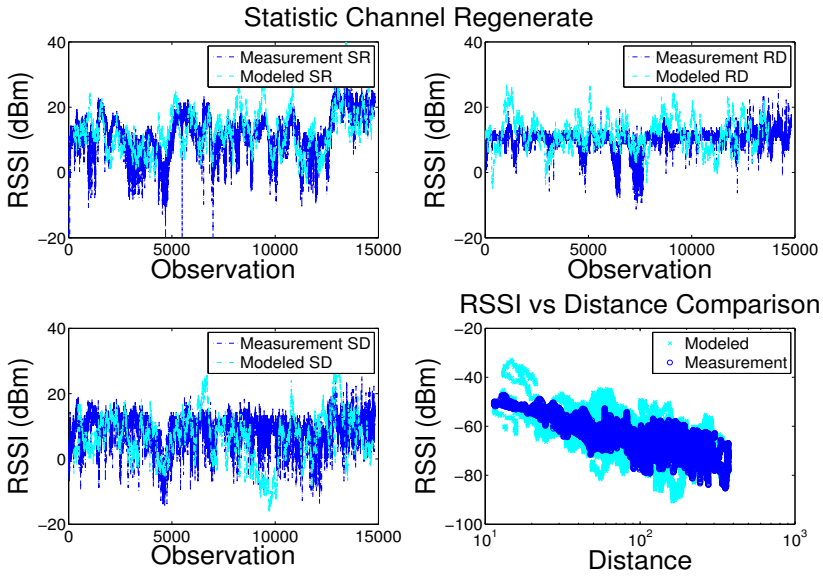

Figure 4.7: Statistic model channel simulation

In Figure 4.7, all modeled RSSI values are demonstrated in cyan color while the mea-

surements RSSI values are the blue ones. In general, the modeled channel characteristics follow the measurements, especially for the SR and SD links comparing the power mean and the deviation of the large scale fading. In the RD link, the fluctuation of the modeled channel appears to be more intensive.

For a Gaussian large scale fading, with a single slope regression pathloss model, the deviation of the SR and RD links is expected to be much higher than in the measurements. One reason for that is, most of the observations in the SR and RD links are in the LOS scenario, and the pathloss in LOS could be better modeled in a dual-slope with a clear multi-ray behavior as mentioned before in section 4.1 pathloss model LOS and OLOS. The neglect of the different behavior in pathloss model would lead to a rougher estimation on the deviation of the large scale fading. These effects are not clearly seen in the SD link since most observations of the SD link are in OLOS scenario.

With the implementation of the correlated Gaussian approach, the behavior caused by the loosen estimation on the large scale fading deviation is restrained with proper correlation characterization. However there is still intensive fluctuation for the RD link. One prediction of the reason is that, the decorrelation distance used in the model is an overall average value for all links, however in the RD link, the used overall decorrelation distance for LOS (150) is much smaller than the averaged value for the RD link itself (200), which leads to a more intensive fluctuations for the simulated channel.

4.4 Packet error rate simulation

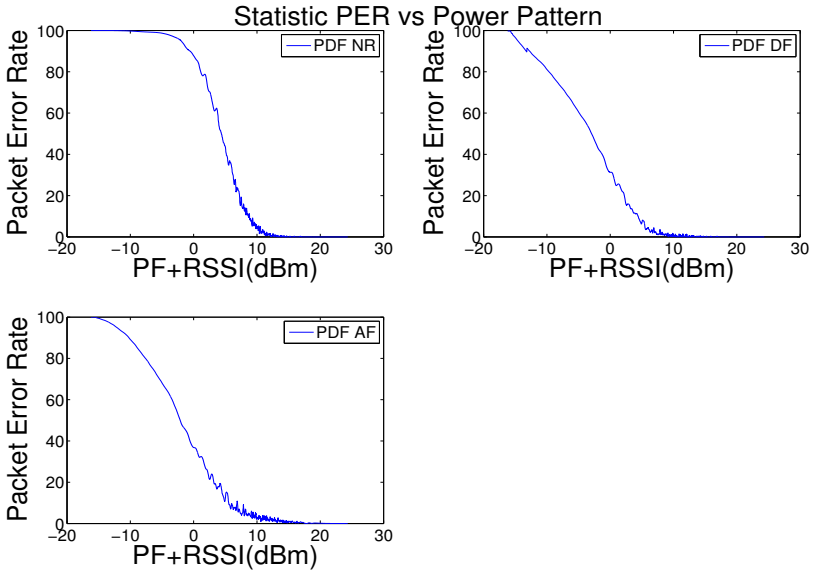

Figure 4.8: Statistic model PER vs power pattern

Based on the results from all the simulations with various power factors, information about simulated packet error rate at certain channel RSSI value regarding the three relay-

ing schemes, Non-relaying (NR), Decode-and-Forward (DF) and Amplify-and-Forward (AF) are well observed (i.e. PER vs Power pattern). After sorting the results by power and deploying several sliding windows, the PER vs Power pattern can be constructed and it is illustrated in Figure 4.8.

With this pattern derived from the simulation results, the simulated packet error rate result can be directly read from it corresponding a modeled channel power. Then the packet error rate performance of the simulated channel could be directly derived based on the simulation channel power regarding the chosen relaying scheme. An example of simulated packet error rate performances for all relaying schemes is demonstrated in Figure 4.9.

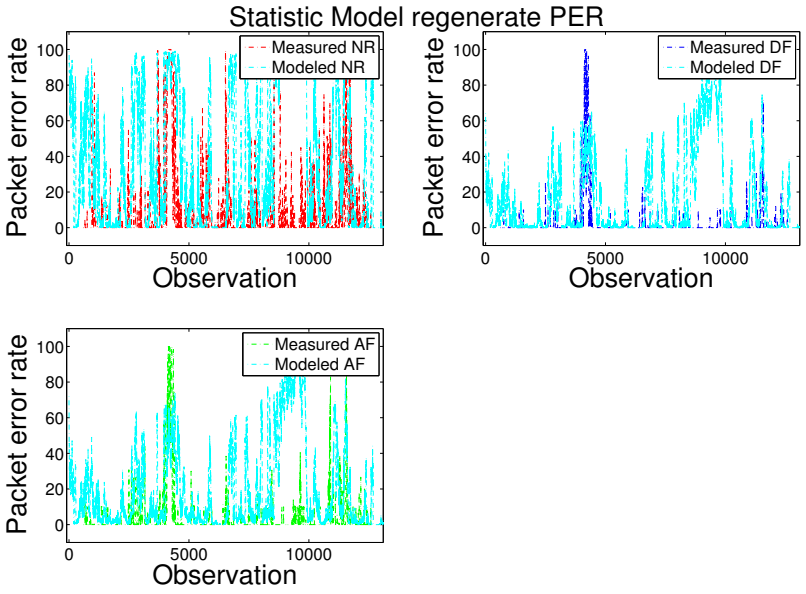

Figure 4.9: Statistic model simulation PER vs observation

As can be seen, the simulated packet error rate of all schemes induced by the derived pattern (cyan) are generally higher than the original simulated results (with power factor 3×10^7). This could be mainly cause by the lower estimation on the channel power of OLOS scenario based on the maximum likelihood estimation as discussed before. The non-relaying link is basically the SD link itself and most observations of the SD link are in OLOS scenario. As previously mentioned, the OLOS scenario has more censored data and the curve of the maximum likelihood estimation at far distances deviates more from the measured data set. As a result, the channel power of the simulation at far distances is generally weaker than the measured channel power. For example in the SD link, the distances between cars are on average over 100 meter and sometimes even reach 300 meter. When distance between cars is larger than 100 meter, the modeled pathloss curve gradually goes beneath the measurements data which leads to a lower power simulation, and consequently a higher packet error rate. This can be observed from Figure 4.2.

Chapter 5

Stochastic Sum of Sinusoids Model

In this chapter, the joint correlation of vehicular shadowing affected by multi-link movement is first studied and a temp stochastic model of shadowing simulation is created based on the sum of sinusoids approach discussed in [18] and [8]. In this thesis, the vehicular channel is treated as an extension of the WSSUS channels. The auto correlation of the shadowing at the transmit vehicle and the receive vehicle are assumed to be independent and modeled with a negative exponential. A Monte Carlo method is used to generate the random spatial frequencies based on the channel power spectral density as discussed in section 2.4 and 2.5. After that, the joint correlation of vehicular shadowing affected by the vehicle distance between two cars under the same obstruction vehicle is studied. The correlations for different distance intervals are evaluated and modeled as negative exponential. This joint correlation property is later added to the sum of sinusoids stochastic model. Finally, the model results are analyzed in the last section.

5.1 Joint correlation with movement

As mentioned in Chapter 2.1.6, the vehicular shadowing is assumed to be an ergodic process while any duration of the process can describe the average statistics of the entire process. Therefore it can be treated stationary within certain observation period. Then as discussed in Chapter 2.5, an stationary Gaussian process could be approximately represented by the sum of finite number of sinusoid waves with random phases and proper chosen frequencies. Lastly in section 2.4, the auto correlation of the multi-link shadowing affected by positions can be modeled as two independent negative exponential which could extend the sum of sinusoids (SOS) stochastic model to 4-dimensional (4D) regarding the shadowing power spectral density.

The movements of the multi-link cars are represented by assigned coordinates which are the input to the 4D model. An example picture of shadowing simulation regarding movement is demonstrated in Figure 5.1 using a discrete Monte Carlo method.

As can be seen from Figure 5.1, the X axis and Y axis represent 2-dimensional (2D) movements for the first car of the multi-link while the other car's coordinates are fixed. The start coordinates of the first car are set to (1, 1) and increase with the car movements in both dimensions. The employed decorrelation distances for both direction are 350 meter based on the calculation results of the measurements. The simulation movement boundary is one thousand for both dimensions.

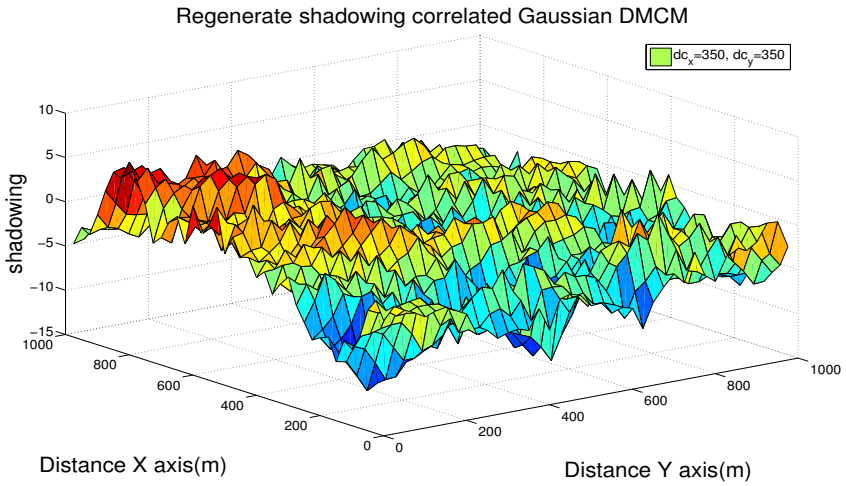

Figure 5.1: Shadowing simulation for 4D position with discrete Monte Carlo method (DMCM)

5.2 Correlation dependence on car distance

In order to study the joint correlation of the vehicular large scale fading affected by the distance between the two receiver vehicles under the same obstruction car, the large scale fading and car distances for all related multi-link pairs are derived first. Figure 5.2 shows an example of a studied multi-link pair in scenario 1b.

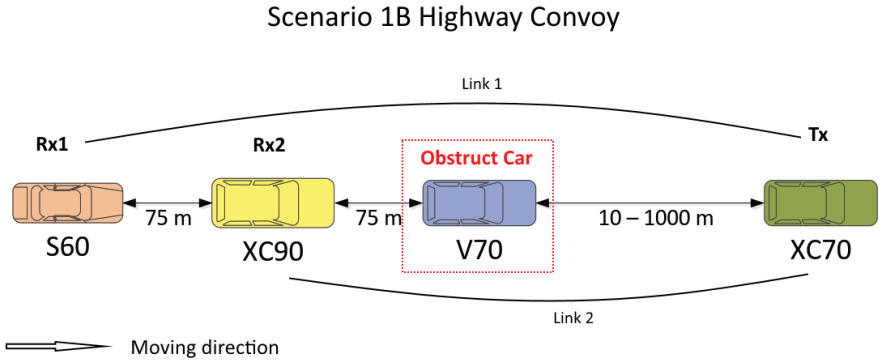

Figure 5.2: Example joint correlation multi-link pair, Scenario 1b

In the convoy scenario 1b, the leading car XC70 (TX) is transmitting to both S60 (RX1) and XC90 (RX2) simultaneously. The second car in queue, V70, is treated as a common obstruction car for both link 1 and link 2. The joint correlation of the large scale fading on the RX1 and the RX2 can be studied based on the distance between RX1 and RX2 disregarding the distances for link 1 and link 2.

Moreover, the roles of the vehicles in the scenario are inverted, treating S60 as the TX and XC90 as the obstruction car. Thereby another related scenario can be observed as 1b reverse. With the same concept, two more related scenarios from convoy 1a can be inspected.

5.2.1 Shadowing versus distance

In order to derive the large scale fading of the desired multi-link pairs, the values of RSSI and distance are first synchronized based on the measured time stamps. Secondly, periods with large packet loss are removed. By subtracting the distance dependent mean based on the pathloss model, the effective large scale fading of the multi-link pairs are calculated. Example derivations of the RSSI values, the distances between cars and the large scale fading are demonstrated in Figure 5.3.

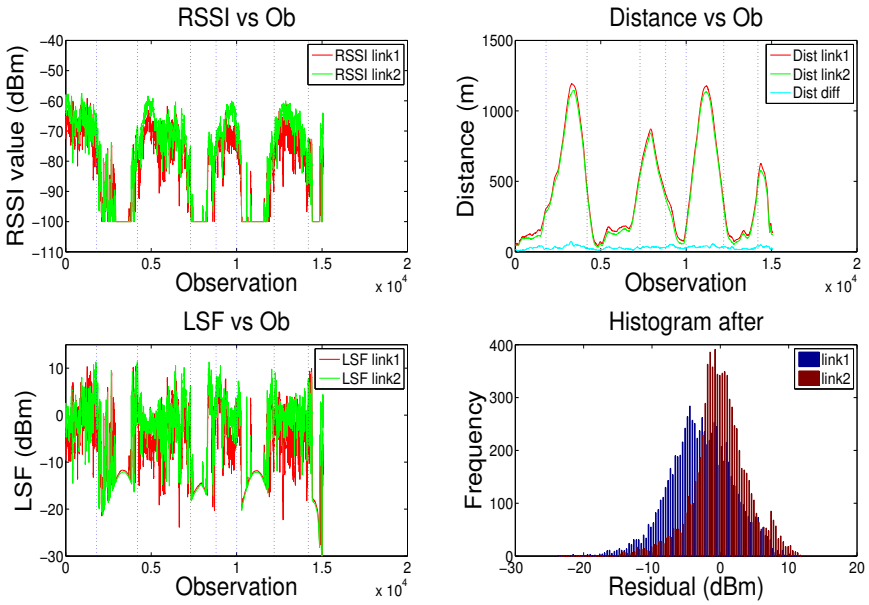

Figure 5.3: RSSI and LSF with extend data

As can be seen in Figure 5.3, the RSSI values, the distances and the large scale fading of the multi-link are plotted including the observations where no packet is received. The red lines represent link 1 and the green ones represent link 2. Then the observation periods of which the RSSI values are mostly unreceived, are removed corresponding to the large distances between TX and RX. After the modification, the large scale fading values are derived by subtracting distance dependent means from the filtered RSSI values. Which the means were taken from the pathloss model for all measurements data disregarding the LOS or OLOS scenario. Finally, the histogram of the result large scale fading is shown in last subfigure indicating a Gaussian distribution. The modified multi-link RSSI values for scenario 1b and pathloss model can be observed from Figure 5.4.

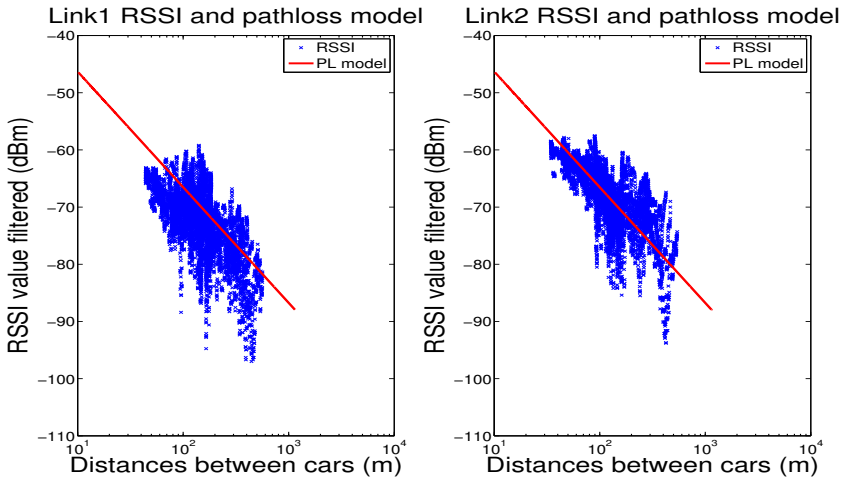

Figure 5.4: Pathloss model and RSSI value, Scenario 1b

To study the large scale fading affected by distances between the two cars of the multi-link pair, the large scale fading versus the distance is derived and illustrated in Figure 5.5. From the figure we can observe that, most of the large scale fading data pairs fall into distance interval 10 to 80 meter. The scatter plot for each 10 meter interval is derived from 10 to 80 meter in consideration of the GPS offset being several meters. An example scatter plot is shown in Figure 5.6 for the 30 to 40 meter interval in scenario 1b. A clear positive correlation with the two large scale fading of the multi-link pair could be observed. A sample reflective correlation coefficient is calculated for each interval to evaluate the joint correlation and it is introduced in next subsection.

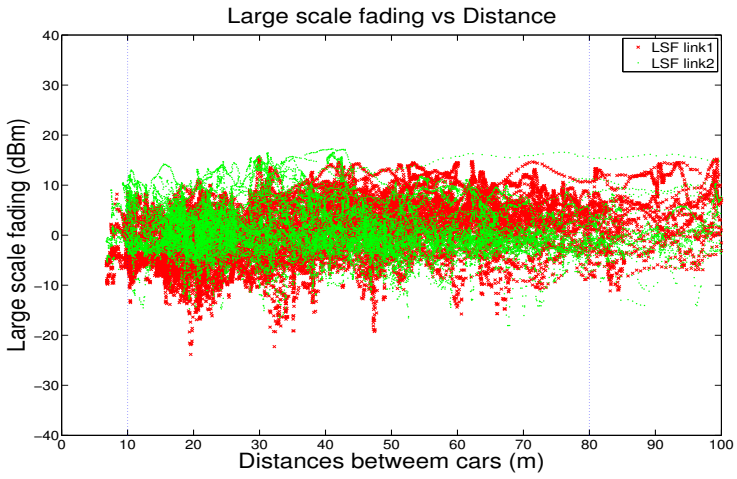

Figure 5.5: Large scale fading vs Distance between cars

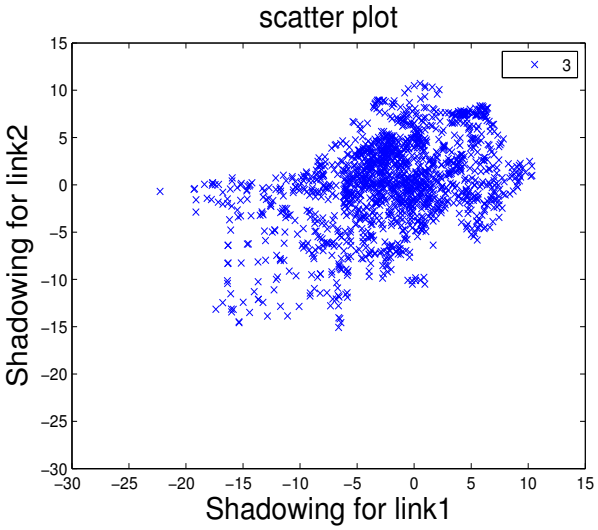

Figure 5.6: Scatter plot, Scenario 1b 30 to 40 meter interval

5.2.2 Sample reflective correlation coefficient

The coefficient of the joint correlation for each distance interval is a description of the correlation between the two large scale fading of the multi-link. Therefore, the means of the two large scale fading are not subtracted during the calculating of the correlation coefficients. A sample reflective correlation coefficient (SRCC) is introduced in equation (5.1),

$$R_{SRCC} = \frac{\frac{1}{N}\sum_{i=1}^{N}\left(x_i \cdot y_i\right)}{\left(\frac{1}{N}\sum_{i=1}^{N} x_i^2\right)^{\frac{1}{2}}\left(\frac{1}{N}\sum_{i=1}^{N} y_i^2\right)^{\frac{1}{2}}}, \tag{5.1}$$

where x and y represents the large scale fading data of the two studied links and N is the number of samples. Eventually, the sample reflective correlation coefficients R_{SRCC} for every 10 meter interval from 10 to 80 meter are calculated. All four scenario data and the results from all four scenarios are combined and illustrated in Figure 5.7.

As can be seen in Figure 5.7, the sample reflective correlation coefficient values are plotted at the middle of the corresponding distance interval. All the values here are positive and indicate a clear descend trend till 80 meter besides the first two points of which the distances are smaller than 30 meter.

The multi-link shadowing data for this studies are measured under a highly dynamic situation. Each pair of the large scale fading are collected under the same time instance. However the position of the obstruction car in the convoy, the distances between transmitting car and receiving cars, and even the antenna heights and the environments of surrounding are essentially different between the data pairs of different observations. The analyzed results could be strongly affected by the measurement environment. With these in mind, the joint correlation of large scale fading affected at different distances from same obstruction car can be observed on an indistinct level.

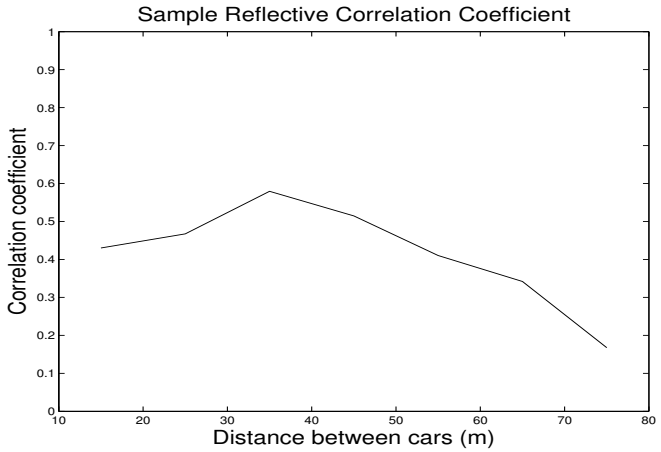

Figure 5.7: SRCC vs Distance

Under such conditions, based on the behaviors of the distance interval 10 to 30 meter, it is assumed that there is a close-vehicle-distance before 30 meter distance, where the large scale fading is mainly affected by the factors other than the car distance, such as the car type, the antenna pattern, the antenna height, etc.

Furthermore, based on the results of sample reflective correlation coefficient, the descend trend can be modeled either linearly or exponentially. In this thesis, the joint correlation of the large scale fading affected by distances between cars is modeled as a negative exponential and it drops from 1 at zero meter. All other influences during the distance interval of 30 to 80 meter are assumed to be neglectable for this particular study object.

5.3 Analysis results

As mentioned in the last section, the sample reflective correlation coefficients (SRCC) from 10 to 30 meter intervals are eliminated and the joint correlation at zero meter is 1. After a proper exponential fit based on the sample reflective correlation coefficient results from 30 to 80 meter intervals, the decorrelation distance of the large scale fading affected by distances between cars is derived based on equation (2.14). Finally, the result is calculated to be 52 meter. The fitting is illustrated in Figure 5.8,

The joint correlation of the large scale fading affected by car distance is now modeled by a negative exponential, which is in the form of the movement factor. It is assumed that this joint correlation with car distance is independent with the correlation with movement. Then based on the same concept of equation (2.25) and equation (2.26), the joint correlation affected by the car distance can be added to the sum of sinusoids model.

For the stochastic sum of sinusoids (SOS) model, the movement of the multi-link vehicle pair is considered as one entirety. The 4D movement SOS model is reduced to a two dimensional model with decorrelation distance of 350 meter on both dimensions. On the other hand, another two dimensions with the decorrelation distance of 50 meter are added representing the car distance effects. Eventually, a 4-dimensional sum of sinusoids shadowing model is created which could be expressed with equation (2.32), and its spatial

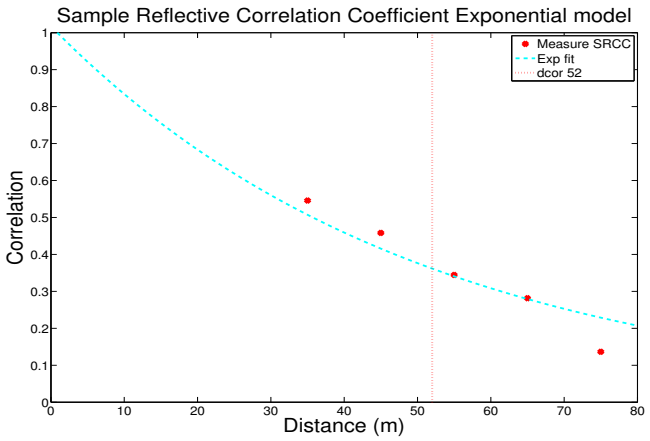

Figure 5.8: SRCC, Exponential fit

frequencies for movement and car distance are generated separately based on equation (2.31) using $a = 350$ and $a = 50$ respectively. An example of the shadowing simulation based on the stochastic SOS model with a Monte Carlo method is demonstrated in Figure 5.9.

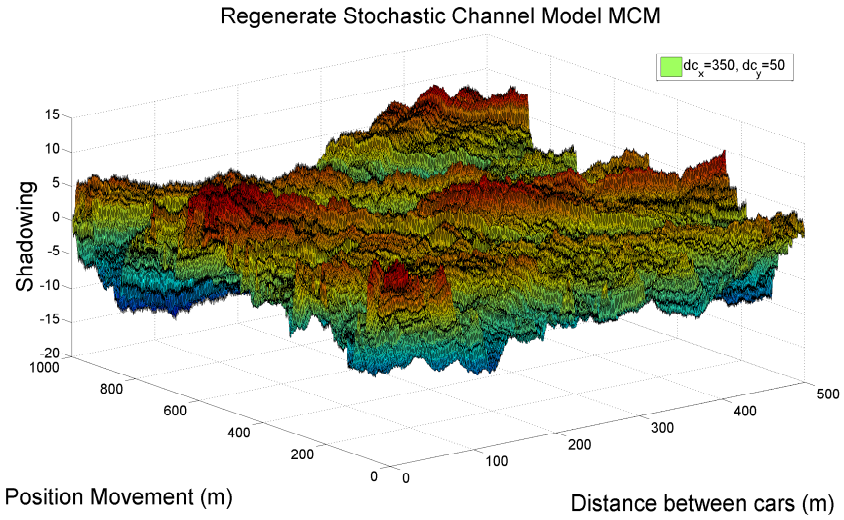

Figure 5.9: Stochastic model shadowing simulation, Monte Carlo

As can be seen from Figure 5.9, the left axis represents the movement of convoy from reference (1, 1) to (1000, 1), the joint correlation spatial frequencies are generated with the decorrelation distance 350 meter. The right axis demonstrates the distance between the two cars of the multi-link pair, with coordinates from (1, 1) to (500, 1). The decorrelation distance for the distance factor is 50 meter.

The shadowing results of the stochastic model could be limited by the accuracy of the pathloss model, the limitation on data size, the valid distance and the GPS offset. In addition to that, the car link with a further distance also suffers an additional blockage from the closer link cars.

Chapter 6
Conclusion

This thesis focuses on the study of vehicular shadowing in multi-link V2V systems. Together three parts compose the main structure: 1) Implemented two relaying schemes, Decode-and-Forward and Amplify-and-Forward, in the simulation based on the measurement data. The packet error rate performance is analyzed; 2) Generate a statistic pathloss and shadowing model regarding the line-of-sight (LOS) and the obstruction LOS (OLOS) scenarios. Simulated the power and PER performance of the channels based on the model and the simulation results; 3) Employ the sum of sinusoids approach for the stochastic shadowing model, based on the joint correlation affected by movements and distance between vehicles under same obstruction car.

The results of the relaying simulations based on the practical measurements indicate that implementing multi-hop technology could effectively solve the issues with shadowed cars. The bit level simulation with Rician distributed channel power is very close to practice and the basic principles of Decode-and-Forward and Amplify-and-Forward schemes are well fulfilled. As for the packet error rate results, Decode-and-Forward and Amplify-and-Forward suggest a significant benefit comparing with the non-relaying. In the meanwhile, the Decode-and-Forward always outperforms the Amplify-and-Forward under the condition that both of the transceivers are transmitting under unit power.

The statistic pathloss and shadowing model well describes the power properties of the measured highway scenarios and can be used to simulate channel power based on distance between transmitters and receives. The implementation of the maximum likelihood estimation makes a better evaluation of the practical signal power loss taking into consideration of the missing packets. The correlated Gaussian model of the vehicular shadowing could better describe the spatial correlation on the measured highway scenario. The pathloss and shadowing model closely characterizes the measured channels with the desired deviations of large scale fading and a close mean pathloss. This model could be used for system level V2V studies under similar highway scenarios.

The joint correlation of vehicular shadowing affected by positions and by distance between vehicles under same obstruction car are modeled as negative exponential. A close distance range should be studied separately. The stochastic sum of sinusoids model for generating Gaussian shadowing well describes the power spectral density and join correlation effects of the multi-link car pairs. Therefore it could be used for multi-link vehicular shadowing simulation on V2V systems based on the vehicle movements and the distance between the vehicles under same obstruction car.

Chapter 7

Discussion and Future Work

As a step forward in deeper studies, this thesis includes several topics about multi-link modeling in V2V channels, involving relaying simulation design, channel statistics derivation and stochastic channel modeling. There could still be several improvements in the details while the major concepts are included in the report.

A single-hop relaying scenario is employed in the simulation. Multi-hop systems with more nodes could be studied, from which more joint correlation properties could be studied for the multi-link shadowing. Furthermore, hybrid and cooperative relaying schemes precisely designed for V2V communication could be employed in the simulation.

The pathloss in this thesis is modeled with the single-slope linear regression. As mentioned in Chapter 4, advanced pathloss models could be applied for the multi-ray and dual-slope behaviors on the line-of-sight scenario. With more accurate prediction of the mean power, the simulated channels would be more close to the measured ones. Moreover, for the convoy situation, in total the data of six links out of twelve are analyzed. More links could be resolved and included in the modeling to increase the accuracy.

The basic linear pathloss model of the multi-link shadowing in this report is based on the assumption that the power loss is independent on the pair of links. This assumption is not absolutely accurate as the power loss of some links can be highly correlated through the shadowing effect, for example, two vehicles suffering correlated shadowing from the same obstruction. Further studies could be made with consideration of a joint pathloss model mentioned by P. Agrawal and N. Patw [9].

In addition to that, the channel could be modeled more comprehensively with the information of frequency domain provided by channel sounders. One can study from elementary channel characteristics like the power delay profile, the power spectral density, the delay spreads, the Doppler spreads, etc.; Directional information could also be analyzed from derivation of the direction-of-arrival (DOA) and direction-of-departure (DOD); The optimal usage of antenna diversity can be evaluated based on the eigenvalue derivation.

Furthermore, only small size vehicles are used in the measurements of this thesis. Similar multi-link studies could be done on large vehicles such as trucks and buses. The multi-link correlation properties should be properly modeled to be able to design V2V systems based on multi-hop technology with low latency and high reliability.

Finally, the study method of collecting channel gain in V2V channels from synchronized transceivers is quite practical, and the parameters needed for the channel modeling are uncomplicated. With the gradually implementation of employing single antenna on

vehicles, there could also be local geometric-based self-tuning channel models, feeding by the channel data of RSSI values, GPS coordinates and synchronized time stamps from the massive passing vehicles. Furthermore, more elements could be taken into consideration, such as vehicle type, vehicle speed, traffic timing, weather, etc. These models could be quickly developed and auto-superseded. They could compensate the effects of environmental changes like new constructed buildings and bridges, growing roadside trees, etc.

Bibliography

[1] A. Paier et al. “Characterization of Vehicle-to-Vehicle Radio Channels from Measurements at 5.2 GHz”. English. In: *Wireless Personal Communications* 50.1 (2009), pp. 19–32. ISSN: 0929-6212. DOI: 10.1007/s11277-008-9546-6. URL: http://dx.doi.org/10.1007/s11277-008-9546-6.

[2] “Vehicle-to-Vehicle Communications: Readiness of V2V Technology for Application”. In: *Report No. DOT HS 812 014* (2014).

[3] C. Gustafson. “60 GHz Wireless Propagation Channels: Characterization, Modeling and Evaluation”. PhD thesis. Lund University, 2014, p. 244. ISBN: 978-91-7623-183-8.

[4] C.F. Mecklenbrauker et al. “Vehicular Channel Characterization and Its Implications for Wireless System Design and Performance”. In: *Proceedings of the IEEE* 99.7 (July 2011), pp. 1189–1212. ISSN: 0018-9219. DOI: 10.1109/JPROC.2010.2101990.

[5] T. Abbas. “Measurement Based Channel Characterization and Modeling for Vehicle-to-Vehicle Communications”. PhD thesis. Lund University, 2014, p. 215. ISBN: 978-91-7473-853-7 (pdf).

[6] M. G. Nilsson et al. “On Multilink Shadowing Effects in Measured V2V Channels on Highway”. In: *Antennas and Propagation (EuCAP), 2015 9th European Conference on*. Apr. 2015, pp. 1–5.

[7] D. Vlastaras et al. “Impact of A Truck as An Obstacle on Vehicle-to-Vehicle Communications in Rural and Highway Scenarios”. In: *Wireless Vehicular Communications (WiVeC), 2014 IEEE 6th International Symposium on*. Sept. 2014, pp. 1–6. DOI: 10.1109/WIVEC.2014.6953226.

[8] W. Zhenyu, E.K. Tameh, and A.R. Nix. “Joint Shadowing Process in Urban Peer-to-Peer Radio Channels”. In: *Vehicular Technology, IEEE Transactions on* 57.1 (Jan. 2008), pp. 52–64. ISSN: 0018-9545. DOI: 10.1109/TVT.2007.904513.

[9] P. Agrawal and N. Patwari. “Correlated Link Shadow Fading in Multi-hop Wireless Networks”. In: *Wireless Communications, IEEE Transactions on* 8.8 (Aug. 2009), pp. 4024–4036. ISSN: 1536-1276. DOI: 10.1109/TWC.2009.071293.

[10] H. W. Ben, A. El Gares, and N. Hamdi. “Resource Management for Amplify and Forward and Decode and Forward Relaying Systems”. In: *Symbolic and Numerical Methods, Modeling and Applications to Circuit Design (SM2ACD), 2010 XIth International Workshop on*. Oct. 2010, pp. 1–4. DOI: 10.1109/SM2ACD.2010.5672351.

[11] M. Andreas. “Wireless Communications”. In: (2005).

[12] C. Gustafson et al. “Statistical Modeling and Estimation of Censored Pathloss Data”. In: *Wireless Communications Letters, IEEE* PP.99 (2015), pp. 1–1. ISSN: 2162-2337. DOI: 10.1109/LWC.2015.2463274.

[13] M. Gudmundson. “Correlation Model for Shadow Fading in Mobile Radio Systems”. In: *Electronics Letters* 27.23 (Nov. 1991), pp. 2145–2146. ISSN: 0013-5194. DOI: 10.1049/el:19911328.

[14] H.M. El-Sallabi. “Fast Path Loss Prediction by Using Virtual Source Technique for Urban Microcells”. In: *Vehicular Technology Conference Proceedings, 2000. VTC 2000-Spring Tokyo. 2000 IEEE 51st*. Vol. 3. 2000, 2183–2187 vol.3. DOI: 10.1109/VETECS.2000.851659.

[15] M. Deserno. “How to Generate Exponentially Correlated Gaussian Random Numbers”. In: (2002). URL: https://www.cmu.edu/biolphys/deserno/pdf/corr_gaussian_random.pdf.

[16] C.F.F. Karney and F.W. Bessel Deakin R.E. “The Calculation of Longitude and Latitude from Geodesic Measurements. Astron. Nachr.” In: 331.8 (Sept. 2010), pp. 765–861. DOI: 10.1002/asna.201011352.

[17] F. Wei et al. “Rician Channel Modeling for Multiprobe Anechoic Chamber Setups”. In: *Antennas and Wireless Propagation Letters, IEEE* 13 (2014), pp. 1761–1764. ISSN: 1536-1225. DOI: 10.1109/LAWP.2014.2352372.

[18] C. Xiaodong and G.B. Giannakis. “A Two-dimensional Channel Simulation Model for Shadowing Processes”. In: *Vehicular Technology, IEEE Transactions on* 52.6 (Nov. 2003), pp. 1558–1567. ISSN: 0018-9545. DOI: 10.1109/TVT.2003.819627.

[19] L. Bernado et al. “Multi-dimensional K-factor Analysis for V2V Radio Channels in Open Sub-urban Street Crossings”. In: *Personal Indoor and Mobile Radio Communications (PIMRC), 2010 IEEE 21st International Symposium on*. Sept. 2010, pp. 58–63. DOI: 10.1109/PIMRC.2010.5671774.

[20] C. Sommer, S. Joerer, and F. Dressler. “On The Applicability of Two-Ray Path Loss Models for Vehicular Network Simulation”. In: *Vehicular Networking Conference (VNC), 2012 IEEE*. Nov. 2012, pp. 64–69. DOI: 10.1109/VNC.2012.6407446.